Astroparticle Physics 35 (2012) 277–286

Contents lists available at SciVerse ScienceDirect

Astroparticle Physics

journal homepage: www.elsevier.com/locate/astropart

Influence of microscopic particle interaction models on the flux of atmospheric antiprotons

Arunava Bhadra [a], Biplab Bijay [a], Sanjay K. Ghosh [b,c], Partha S. Joarder [c], Sibaji Raha [b,c,*]

[a] High Energy & Cosmic Ray Research Centre, University of North Bengal, Siliguri 734013, West Bengal, India
[b] Department of Physics, Bose Institute, 93/1 A.P.C. Road, Kolkata 700009, India
[c] Centre for Astroparticle Physics and Space Science, Bose Institute, Block EN, Sector V, Salt Lake, Kolkata 700091, India

ARTICLE INFO

Article history:
Received 18 February 2011
Received in revised form 30 July 2011
Accepted 12 September 2011
Available online 25 September 2011

Keywords:
Antiproton
BESS observations
Particle interaction models
PAMELA experiment

ABSTRACT

We study the effect of particle interaction models on the theoretical estimates of atmospheric antiproton flux by comparing the BESS observations of antiproton spectra with the spectra obtained by means of a full three dimensional Monte Carlo simulation program. For such a purpose, we use two popular microscopic interaction models, namely FLUKA and UrQMD, to simulate antiproton spectra at multiple observation levels. In this article, we further compare the atmospheric antiproton fluxes predicted by a few popular microscopic high energy particle interaction models with each other to get an idea about the influence of such models at energies beyond the BESS upper cutoff up to about 100 GeV. We find that the simulated antiproton flux has strong dependence on the choice of interaction models. The present analysis seems to further indicate that the theoretical prediction of galactic antiproton spectrum may be uncertain by an appreciable amount due to our limited knowledge of particle interaction characteristics.

1. Introduction

Antiprotons ($\bar{p}$) in cosmic rays are supposed to provide information on the sources of cosmic rays and their propagation in the Galaxy as well as the matter–antimatter asymmetry of the local universe [62]. They are also believed to play crucial role in indirect dark matter search [23,53,56]. Primary $\bar{p}$ may as well be produced from the evaporation of primordial black holes (PBH) [47,57]. Observations of $\bar{p}$ spectrum with appropriate features may, therefore, be considered for probing into the possible signatures of the PBH.

Recently, the PAMELA instruments attached to the Russian Resurs-DK1 satellite have made a precise measurement of $\bar{p}$ spectrum in the energy range from 60 MeV to 180 GeV [6,8]. Comparison with several theoretical estimates [32,66,75] seems to support the view that the PAMELA $\bar{p}$ spectrum is consistent with a scenario of pure secondary production of $\bar{p}$ *via.* cosmic ray interactions in the interstellar medium (ISM) [6,8].

An accurate estimation of the secondary antiproton flux is, however, a difficult task. This is because of the fact that such an estimate requires precise knowledge of three factors, namely, the detailed features of cosmic ray propagation in the Galaxy, the characteristics of high energy particle interactions and the effect of solar modulation on the cosmic rays. While we have a reasonable understanding of the solar modulation effect, major uncertainties in the predicted flux still arise from our incomplete knowledge of cosmic ray propagation and the high energy particle interactions.

Over the past few years, the BESS experiments have reported the results of the precise measurements of atmospheric $\bar{p}$ spectra in an energy range 0.2–3.4 GeV at three observation levels, namely, the balloon altitude, mountain altitude and the sea level [72,84]. It is interesting to note that the cosmic rays traverse a depth (5–6 g cm^{-2}) of matter in the Galaxy that is close to the average atmospheric depth (10.7 g cm^{-2}) of the BESS-2001 balloon observation at the location of Ft. Sumner, USA [84]. As the $\bar{p}$ production mechanism in the atmosphere is likely to be similar to that in the Galaxy, a study of such atmospheric $\bar{p}$ at balloon altitude would possibly provide us with an opportunity to quantify the uncertainty in the theoretical estimate of interstellar $\bar{p}$ flux that may be caused by our limited knowledge of high energy particle interactions.

A good knowledge of particle interactions in the energy range from sub-GeV to about 100 GeV is required to understand the production and transport of the BESS-detected atmospheric $\bar{p}$s with their energies in the range between 0.2 GeV to a few GeV. Due to the steeply falling energy spectra of the primary cosmic rays, the contribution of primary particles with energies above 80 GeV/n to such BESS-observed atmospheric $\bar{p}$ spectrum has been recently

* Corresponding author at: Department of Physics, Bose Institute, 93/1 A.P.C. Road, Kolkata 700009, India.
E-mail addresses: aru_bhadra@yahoo.com (A. Bhadra), biplabbijay@rediffmail.com (B. Bijay), sanjay@bosemain.boseinst.ac.in (S.K. Ghosh), partha@bosemain.boseinst.ac.in (P.S. Joarder), sibaji@bosemain.boseinst.ac.in (S. Raha).

0927-6505/$ - see front matter © 2011 Elsevier B.V. All rights reserved.
doi:10.1016/j.astropartphys.2011.09.002

found to be insignificant [24]. GHEISHA (version 2002d) [40], UrQMD (version 1.3) [20,25] and FLUKA (version 2008.3b) [21,39] are among the most popular models for describing particle interactions in the relevant energy range. Such models are useful for the study of the development of cosmic ray cascades in the atmosphere. Among the three models mentioned above, GHEISHA is based on the parametrization of accelerator data, while UrQMD and FLUKA describe particle interactions microscopically.

The purpose of the present work is to study the influence of high energy particle interaction models on the atmospheric $\bar{p}$ spectra through the three dimensional Monte Carlo (MC) simulation methods. For such a purpose, we first simulate the atmospheric $\bar{p}$ spectra at multiple observation levels by using FLUKA and UrQMD models and then compare such simulated spectra with the BESS observations. The interaction model GHEISHA is not considered here (except in Fig. 3(b)) as the model is known to have shortcoming in describing fixed target accelerator data as well as the atmospheric cosmic ray data [24,34,49]. The present study is also prompted by the recently reported fact [24] that the BESS-measured atmospheric $\bar{p}$ flux at mountain altitude [72] is substantially less than the simulated flux obtained from FLUKA, while the flux obtained from UrQMD is consistent with experimental measurements. It is important to know whether such a discrepancy between the simulated and the experimental fluxes persists even at a very high (balloon) altitude or at the sea level. Such a study may have important bearing on our understanding of the reasons behind the disagreement between the FLUKA-derived results and the BESS measurements.

We here note that several MC simulations [18,36,51,77,78], relying mostly on phenomenological description of high energy particle interactions, have been carried out in the past to study the atmospheric $\bar{p}$ spectra. Such an approach does not usually satisfy many of the conservation laws in a single hadronic interaction and also suffers from various other inconsistencies (see, for instance, [27]). Besides, an understanding of the atmospheric $\bar{p}$ production also requires a good estimation of cosmic ray secondaries (mostly protons) in the atmosphere that was not considered in many of such earlier studies. In the present study, we further take the residual effect of the galactic $\bar{p}$ flux at the observation level into consideration that was mostly ignored in the calculations mentioned above.

The BESS-measured $\bar{p}$ spectra are limited to 3.4 GeV that corresponds to the mean vertical geomagnetic rigidity cutoff at the location of Ft. Sumner, USA. A simulation study of atmospheric $\bar{p}$ at very high altitude, that corresponds with the BESS observations at Ft. Sumner, is therefore relevant only for the low energy end of the galactic $\bar{p}$ spectrum measured by the PAMELA experiment [6,8]. To simulate the atmospheric $\bar{p}$ flux up to about 100 GeV, a good understanding of particle interactions up to at least a few hundred GeV is necessary. Due to the paucity of experimental data [35] on the inclusive $\bar{p}$ production and annihilation cross sections over the whole kinematic region in hadron–hadron, hadron–nucleus and nucleus–nucleus collisions in the stated energy range, one has to strongly rely on various theoretical models of particle interactions. In the absence of experimental data, we here compare the predictions of the well known high energy interaction models QGSJET (version 01c) [55], VENUS (version 4.12) [82], NEXUS (version 3.97) [33,67] and EPOS (version 1.6) [83], each in combination with FLUKA (version 2008.3b) for the description of hadronic interactions below 80 GeV/n, to get some idea about the theoretical uncertainties in the predicted $\bar{p}$ flux at energies beyond the upper cutoff for the BESS-2001 balloon experiment, i.e., over an energy range of about 3–100 GeV.

In a recent work [24], we found that the atmospheric proton spectrum, as measured by the BESS detector at mountain altitude [72], may be reasonably described by the FLUKA model; whereas, the model UrQMD works well at relatively higher energies. Such a proton flux deep in the atmosphere results from the production of protons in the interactions of primary/secondary cosmic rays with air nuclei as well as the absorption of such protons during their propagation through the Earth's atmosphere. Secondary proton spectrum at very high altitude, on the other hand, is likely to contain cleaner information on proton production alone. As the major fraction of such secondary protons arises from hadronic interactions in the forward kinematic region, a study of such proton spectra at very high altitude is likely to provide us with an opportunity to investigate particle production in the forward region. As a continuation of our study in [24], we therefore examine the dependence of atmospheric proton flux at balloon altitude on various hadronic interaction models in this article apart from the study of such a dependence on the atmospheric $\bar{p}$ spectrum as is already mentioned in the previous paragraphs.

Apart from the ambiguity in high energy particle interactions, a dominant systematic error in evaluating the flux of cosmic ray secondaries arises from the uncertainties involved in the estimation of input fluxes of primary cosmic rays. To minimize such uncertainties, spectra of different primary particles measured by the BESS-98 experiment [71] are used as the inputs in our simulations such that the systematic errors in the calculation of atmospheric fluxes are nearly eliminated as we compare with the BESS experimental fluxes of atmospheric protons/antiprotons at different altitudes.

The plan of the article is outlined as in the following. In the next section, we briefly describe the production mechanisms of $\bar{p}$ in high energy collisions and the ways in which different models implement such mechanisms. In Section 3, we give a brief description of the adapted simulation technique. In Section 4, we present the results of our MC simulations. Summary and discussion are presented in Section 5.

2. Production and transport of antiprotons in the atmosphere

2.1. General aspects

Antiproton flux in the atmosphere relies mainly on two factors, namely, the inclusive $\bar{p}$ production cross section in cosmic ray-air nuclei collisions and the propagation of $\bar{p}$ in the atmosphere. The latter factor also includes ionization energy loss, loss of $\bar{p}$ due to annihilation and other interactions.

Antiprotons are produced in the atmosphere in high energy interactions of primary and secondary cosmic ray hadrons/nuclei with air nuclei. A typical example could be the interaction $p + N \rightarrow \bar{p} + p + p + p + N$ with N representing a nucleon. The threshold proton energy for such interaction is about 6.6 GeV in the rest frame of the target nucleon. In addition to the above interactions, meson-nucleon interactions may also lead to the excitation of color flux tubes and their subsequent decay into baryon–antibaryon pairs.

The final state in high energy hadron–nucleon collisions often consists of many particles. Basic reaction for the production of $\bar{p}$ is, therefore, the inclusive $N + N \rightarrow \bar{p} +$ anything process and the inclusive $\bar{p}$ production cross section is one of the main ingredients for the calculation of atmospheric $\bar{p}$ flux. Such $\bar{p}$ production is likely to take place in the central kinematic region rather than the fragmentation region. Antibaryon absorption can also be important in the case of massive nuclear collisions. The $\bar{p}$ mean multiplicity is the other main input for the $\bar{p}$ production spectrum. For propagation of $\bar{p}$ through the atmosphere, the annihilation cross-section of $\bar{p}$ due to its collisions on light nuclei (N and O) are of primary importance.

In the instant case, several $\bar{p}$ production cross-section data on the collisions of proton with various fixed target nuclei in the

(laboratory) energy range of a few GeV to about 400 GeV are available. A complete data set is, however, available for p, π, and K projectiles at 100 GeV (lab) energy on p, C, Cu, Sn and Pb targets where the momenta of the secondary antiprotons are measured [19]. Apart from such data, some measurements on the $\bar{p}p$ and $\bar{p}C$ collisions in the sub-GeV to hundreds of GeV energy range are also available [1,9,30,52,79]. A semi-phenomenological fit to such data can, therefore, be employed for the calculation of atmospheric $\bar{p}$ flux with some level of accuracy and this has been a popular approach [17,28,76–78] for more than 25 years.

A precise estimation of the atmospheric $\bar{p}$ flux additionally requires reliable estimates for the secondary cosmic ray flux that may, in turn, produce further $\bar{p}$ by colliding with air nuclei. Tertiary $\bar{p}$s (arising from inelastically scattered secondaries) also contribute at low energies. One needs to further consider the residual galactic component of $\bar{p}$ in the case of very high (balloon) altitude.

2.2. Importance of high energy interaction models

Computation of hadron production, particularly at low transverse momenta, is not yet possible from first principles within quantum chromodynamics (QCD). One, therefore, relies on phenomenological models that are appropriately tuned to match with the prevailing experimental data. Even a parametrization of such models may be difficult as the accelerator data for the relevant target-projectile combinations covering the whole kinematic region are not available. Experimental data on hadron–hadron interactions in the forward kinematic region at high energies and the data on hadron–nucleus and nucleus–nucleus interactions at all energies covering the whole kinematic range are particularly scarce. One has to resort to theoretical models of particle interactions in such cases. Microscopic models are preferred over the parametrized inclusive models in view of the preservation of correlations such that the basic conservation laws are maintained at every single interaction level. Moreover, such microscopic models have predictive power in the regions in which experimental data are not available.

Hadronic interactions are well described by resonance production and subsequent resonance decay near the particle production threshold; whereas, such particle production scenario becomes too complex at higher ($E_{lab} > 5$ GeV) energies. In the latter situation, most of the particles are produced with low transverse momenta and, therefore, along the projectile direction so that a very large number of resonances of very short lifetimes have to be considered to describe particle production that may not be possible in practice. Such a difficulty gives rise to a number of attempts to develop various hadronic interaction models. Among such models, the string-based phenomenological models such as the Quark-Gluon Strings (QGS) model [54] and the Dual Parton Model (DPM) [29] are of particular interest as they are found to describe particle production at high energies reasonably well.

2.3. Outline of various particle interaction models

The interaction model FLUKA [21,39] employs resonance superposition from threshold to about 5 GeV but incorporates the two-strings interaction model (DPM) at higher energies. In this model, the resonance energies, widths, cross sections and the branching ratios are extracted from data and from the conservation laws by making explicit use of the spin and isospin relations. For high energy hadron–nucleus interactions, the model exploits the Glauber–Gribov cascade [44,45]; whereas, it uses the pre-equilibrium-cascade model PEANUT [37,38] below about 5 GeV. The nucleus-nucleus interactions above a few GeV/n are treated in FLUKA (version 2008.3b) by interfacing with the DPMJET-III [69] model.

The UrQMD (Ultra-relativistic Quantum Molecular Dynamics, version 1.3) model [25] was originally designed for simulating the relativistic heavy ion collisions in the (center of mass) energy range from around 1 AGeV to a few hundred AGeV for the RHIC experiment. This particular model inherits the basic treatment of the baryonic equation of motion in quantum molecular dynamic approach and describes the phenomenology of hadronic interactions at low to intermediate energies in terms of the interactions between known hadrons and their resonances. The model does not use an intrinsic cross section calculation. Instead, the projectile is allowed to hit a sufficiently large disk involving maximum collision parameters as a result of which the program consumes rather long a CPU time. We may add here that both UrQMD and FLUKA describe the fixed-target data reasonably well.

In the string-based models, the high energy nucleonic interactions lead to the excitation of color flux tubes. Antiprotons are produced *via.* the decay of such color flux tubes and also in antiresonance decays; whereas, the $\bar{p}$ annihilation is modeled *via.* the annihilation of quark-antiquark pairs and the formation and subsequent decay of two color flux tubes with baryon number zero. The annihilation of baryon–antibaryon pairs proceeds in UrQMD according to rearrangement diagrams. Here, the formation of two $\bar{q}q$-strings of equal energies in the c.m. system is assumed, while the remaining constituent quarks are rearranged into newly produced hadrons.

At higher energies, the interactions of nucleons and nuclei are calculated on the basis of the Gribov–Regge theory [43] that describes the observed rise of cross-sections at high energies as a consequence of the exchange of multiple supercritical Pomerons [16]. All observed scattering processes are successfully described with the Reggeon–Pomeron scattering scheme [16]. Presently, the Gribov–Regge theory-based interaction models used for cosmic rays include the QGSJET 01c [55], VENUS 4.12 [82], DPMJET-III [69], NEXUS 3.97 [33,67] and the EPOS 1.6 [83] models. Such different models in this class differ from each other in the details concerning the precise formulation of string formation and decay, treatment of the remnants, etc.

Being based on the quark-gluon string description of high energy interactions, the QGSJET model treats the hadronic and nuclear collisions in the framework of Gribov's Reggeon approach [44] as the multiple scattering processes. The individual scattering contributions are phenomenologically described in this model as Pomeron exchanges. The VENUS model considers color exchange between the quarks as well as the antiquarks. In this model, an individual collision leads to color exchanges between the quarks and between the antiquarks with such color rearrangements being the origin of color string formation. After all the strings have been formed due to color exchanges, they are fragmented into the observable hadrons by using an iterative fragmentation cascade. The fragmentation is assumed to be the same as in lepton scattering. Which nucleons from the projectile and the target nuclei collide with each other is determined from geometrical considerations.

While none of the mentioned models violates important theoretical principles, NEXUS and EPOS are the only models in which the theoretically predicted energy–momentum sharing between the hadron constituents is consistently implemented in the construction of scattering amplitudes. Being based on partons and strings, the NEXUS 3.97 [67] and the EPOS 1.6 [83] models employ the multiple scattering approach through a "three object picture" – a parton ladder between two interacting partons, one of which is from the projectile and the other is from the target, along with two excited colorless remnants formed by the spectator partons of the projectile and the target nucleons. The parton ladder describes successive parton emission through the soft and the hard interactions with the soft interaction being described by the traditional soft Pomeron exchange; whereas, the hard interaction is

realized through perturbative QCD within the concept of the semi-hard Pomeron. According to the number of quarks and antiquarks, to the phase space and to an excitation probability, a remnant decays into mesons, baryons and antibaryons [60]. The remnants produce particles mostly at large rapidities whereas the parton ladders emit particles mainly at central rapidities. Such "three object picture" of the parton-ladder and the two remnants solve the multistrange problem of conventional high energy models [26].

To implement energy conserving multiple scattering, these models consider both the open parton ladders as well as the closed parton ladders. Although the parton ladders of the latter category do not contribute to particle production, they nevertheless play a crucial role in the calculation of partial cross sections through interfering contributions. The NEXUS/EPOS models use relativistic string approach to obtain observable hadrons from partons *via.* two steps, namely, the formation of strings from the partons and then the string fragmentation into hadrons.

Being the successor to NEXUS, EPOS has adopted some additional aspects such as the nuclear effects related to Cronin transverse momentum broadening, parton saturation and screening. The model also puts special emphasis on high parton densities. The particle production scenario is expected to be very different depending on whether the interaction is with a peripheral nucleon or with a nucleon from the high density central part. This aspect has been accomplished in EPOS by allowing splitting (as well as merging) of parton ladders based on an effective treatment of lowest order Pomeron–Pomeron interaction graphs with the corresponding parameters being adjusted from the comparison with RHIC data.

In the case of meson projectile, the EPOS model leads to an increase of baryon and antibaryon production in the forward direction in agreement with the low energy pion-nucleus data [19]. In fact, the EPOS model seems to be the only model used both for EAS simulations and accelerator physics that is able to reproduce almost all the experimental data from 100 GeV lab to 1.8 TeV center of mass energy, including antibaryons, multistrange particles, ratios and p_t distributions.

3. Implementation of the simulations

In the present work, we generate atmospheric cosmic ray proton and antiproton spectra by employing the interaction models FLUKA 2008.3b and UrQMD 1.3 in the framework of the cosmic ray EAS simulation code CORSIKA (version 6.735) [48]. Following the default settings of the CORSIKA code, FLUKA and UrQMD have been used up to 80 GeV/n, while the model QGSJET 01c has been used above such energy threshold. As mentioned in Section 1, we also use the high energy interaction models VENUS 4.12, NEXUS 3.97 and EPOS 1.6, each in combination with the FLUKA model, to compare various theoretical estimates of the atmospheric $\bar{p}$ flux at energies beyond the BESS upper cutoff up to about 100 GeV. Other considerations/settings used in this work are briefly described in the following.

3.1. The primary spectra

Uncertainties in the determination of primary cosmic ray flux have been substantially reduced in recent years due to the precise measurements of such flux by the BESS-98 [71], BESS-TeV [46] and the AMS [10,11] experiments. The observed total primary nucleon flux below 100 GeV/n is found to agree within an accuracy of 4.0% in the above three experiments [41,73]. For such a reason, and considering the fact that we would compare our results with the BESS observations, we choose the BESS-98 spectra as the input primary spectra in our simulations while extending the maximum (kinetic + rest-mass) energy of the primary particles up to 1 PeV/n. For reproducing the BESS-observed primary spectra in CORSIKA, the effect of solar modulation on the spectra has been handled by using the *force field approximation* [42,61] in which the primary particle flux is expressed in terms of a time dependent *solar modulation potential* $\phi(t)$ that takes on different values for different epochs of solar activity [80]. For the BESS balloon-borne measurements of the atmospheric proton and antiproton fluxes in September 2001 at Ft. Sumner, USA [3,4,84], the primary cosmic ray spectra are generated by taking a solar modulation potential $\phi = 891$ MV [80] into account. Again, for the BESS sea-level measurements of the antiproton fluxes [84] at Tsukuba, Japan during 6th–11th May and 7th–13th December 1997, we consider $\phi = 410$ MV [80] as the mean value of the solar modulation potential.

3.2. The geomagnetic rigidity cutoff

The geomagnetic rigidity cutoff calculations have been performed by using the (back) trajectory-tracing technique [74]. The quiescent International Geomagnetic Reference Field (IGRF) model of 1995 [70] for the Earth's magnetic field has been used for such calculations. Both the umbra and the penumbra regions in the rigidity range of a primary particle in any particular direction have been taken into consideration [24] in our treatment of the rigidity cutoff. In Fig. 1, we display the values of the mean geomagnetic rigidity cutoff for the primary cosmic ray particles entering the atmosphere at the location of Ft. Sumner from various directions as an example of our rigidity calculations. Such cutoff calculations are used in the simulations to modify the primary cosmic ray spectra obtained from CORSIKA, although the calculation of the re-entrant albedo cosmic ray flux is not incorporated in the present simulations; see Section 5.

3.3. Other settings

The fluxes of cosmic ray particles also depend on the atmospheric density profile. Such a density profile, in turn, has latitudinal and seasonal variations. The effect of such variations on the atmospheric cosmic ray spectra is, however, expected to be small, particularly in the case of very high altitude observations. We, therefore, consider the US-standard atmospheric model [59] with a planar approximation in the present work.

Proton, helium and the heavier nuclei up to iron are considered here as the primary cosmic ray particles. Instead of taking each of the elements individually, the primary nuclei heavier than helium are taken in three separate groups, namely, medium ($5 < Z < 10$, $\langle A\rangle \approx 14$), heavy ($11 < Z < 20$, $\langle A\rangle \approx 24$) and very heavy ($21 < Z < 30$, $\langle A\rangle \approx 56$) nuclei respectively [24]. The spectra for such groups are taken from the compilation of Ref. [81]. The sum of the fluxes of individual elements in a group is taken as the flux of that particular group and the weighted average value of the power indices of such individual elements is taken as the power index of the group [24].

Particular care should, however, be taken for the simulation of atmospheric antiproton flux at a very high altitude. Such atmospheric antiprotons may, in fact, have significant contribution from the residual galactic $\bar{p}$s arriving at the observation level. In this work, we generate a secondary $\bar{p}$ spectrum by combining the simulation-generated (and normalized to the BESS-98 spectrum) primary proton spectrum with the recent measurement of antiproton to proton flux ratio obtained in the PAMELA experiment [6]. The resultant secondary $\bar{p}$ spectrum, adjusted for the location of Ft. Sumner and for a solar modulation potential appropriate for the BESS-2001 experiment, is considered along with the usual primary cosmic ray particles as the inputs in the simulations. However, the integrated secondary $\bar{p}$ flux is found to be only about $1.4–1.5 \times 10^{-4}$ times the integrated primary proton flux in our

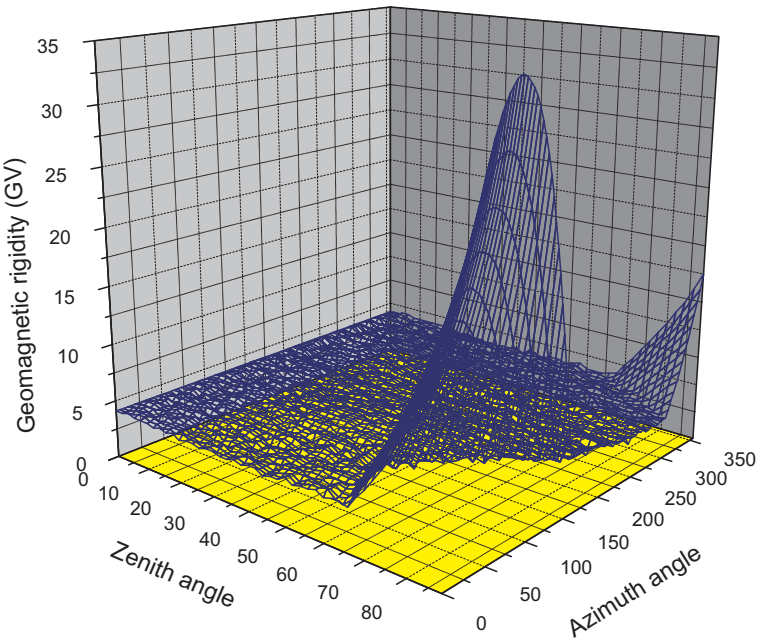

Fig. 1. Directional dependence of the mean geomagnetic rigidity cutoff for primary cosmic rays at the location of Ft. Sumner, USA.

simulations. We have checked that such interstellar $\bar{p}$ flux, in fact, have negligible effects on the generated atmospheric antiprotons within the energy range considered by the BESS experiments and even beyond.

Note that the fluxes of atmospheric shower particles obtained by using CORSIKA have statistical as well as systematic errors. In the present work, nearly 4–20 $\times$ 10^7 events have been generated in each of our simulations for the estimation of the fluxes of atmospheric shower particles, the results of which are presented in the following.

4. Simulated results and comparison with observations

The BESS-2001 experiment [3] is a balloon-borne experiment that was carried out in September 2001 at Ft. Sumner, USA. It consisted of a high resolution spectrometer with a large acceptance capable of performing precise measurements of absolute fluxes of various cosmic rays and their dependence on the atmospheric depth. The secondary proton and helium spectra in an energy range 0.5–10.0 GeV/n and the atmospheric muon spectra in a momentum range 0.5–10.0 GeV/c were measured at atmospheric depths ranging from 4.5 to 28.0 g cm^{-2} during the slow descending period of the balloon flight [3,4]. Atmospheric antiproton flux was also measured in the energy range 0.2–3.4 GeV and, reportedly, at a mean atmospheric depth 10.7 g cm^{-2} [84]. The zenith angle θ_z of the BESS-2001 measurements was limited to $\cos\theta_z \geqslant 0.9$ to obtain nearly vertical fluxes of atmospheric particles [3].

The BESS experiment also measured the sea-level antiproton flux at KEK, Tsukuba during 6th–11th May and 7th–13th December 1997 at a mean atmospheric depth 994.0 g cm^{-2} in the energy range 0.2–3.4 GeV [84].

Fig. 2 depicts the simulated atmospheric proton flux at the location of Ft. Sumner at the atmospheric depths (a) 10.5 g cm^{-2} and (b) 26.4 g cm^{-2}. Corresponding BESS-measurements [3,4] are also shown in the figure. We note that the statistical errors in the simulated spectra are quite small and fall within the widths of the representing lines in Fig. 2.

The BESS-2001-observed proton spectra in Fig. 2 show the following characteristic features. With the increase of energy from about 0.3 GeV, the differential flux initially decreases thus attaining a minimum value at about 2.5 GeV. Such a minimum is followed by an increase in flux up to a maximum at around 3.4 GeV above which the flux decreases again. Above about 2.5 GeV, bulk of the contribution to the observed flux is from primary protons with the peak being due to the geomagnetic cutoff effect. Below 2.5 GeV, the observed spectrum is due to secondary protons produced by the interaction of primary cosmic rays with atmospheric nuclei.

In Fig. 2, we find that the spectra derived from FLUKA and UrQMD models have features similar to those in the measured spectra. Both the models, however, yield fluxes that are lower than the measured values particularly at energies below 1.0 GeV. We also note that the simulated results match better with the measurements at 26.4 g cm^{-2} in Fig. 2(b) than at 10.5 g cm^{-2} in Fig. 2(a).

Fig. 2 shows an additional peak in the UrQMD-derived spectrum at about 1.4 GeV. In this context, we note that the kinetic energy corresponding to the mean vertical geomagnetic rigidity cutoff at Ft. Sumner [84] is also about 1.4 GeV/n for the threshold primary helium nuclei. To investigate if the anomalous peak in the UrQMD-derived flux in Fig. 2 is due to such primary α particles, we plot the separate contributions of (a) primary proton and (b) primary α components to the secondary proton flux in Fig. 3(a) and (b) at an atmospheric depth 10.5 g cm^{-2} at the location of Ft. Sumner. It is clear from this figure that the additional peak in UrQMD in Fig. 2 is indeed contributed by the primary helium nuclei. To check if there is any error in our simulations, we also compute the secondary proton flux from primary α particles in Fig. 3(b) by using the GHEISHA model. We find no additional peak in the GHEISHA model, the result of which is consistent with the FLUKA result. Fig. 3 thus seems to suggest that the fragmentation channel for quasi-elastic interactions between helium and air nuclei is overestimated in the UrQMD model. Such a finding is somewhat unexpected as the UrQMD model was primarily developed to address the nucleus–nucleus interactions and the model is known to well-reproduce the accelerator data. Further study on the stated feature in UrQMD seems, therefore, to be necessary. In Fig. 2, we also note that the results simulated with FLUKA and UrQMD models show very close agreement with each other at low energies, below about 1.0 GeV.

Fig. 4 shows the simulated atmospheric $\bar{p}$ fluxes in comparison with the BESS-measurements at balloon altitude, at mountain altitude and at the sea-level. The bandwidth of each of the bands

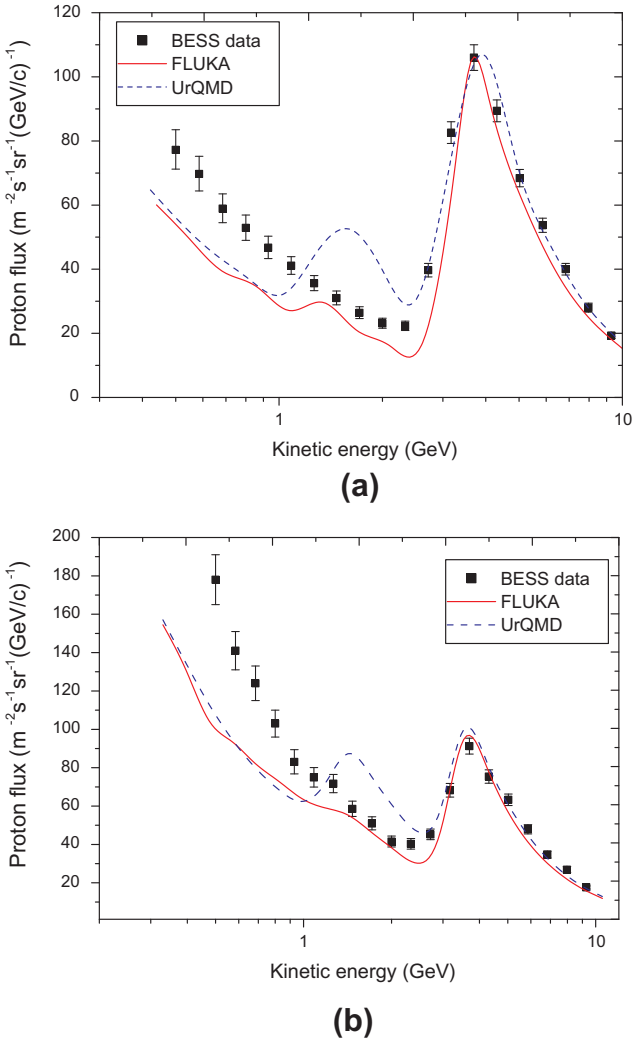

Fig. 2. Differential spectra of vertical atmospheric proton flux at the location of Ft. Sumner, USA that are obtained by using two hadronic interaction models at the atmospheric depths (a) 10.5 g cm^{-2} and (b) 26.4 g cm^{-2}. The results of the BESS-2001 observations at such depths [3,4] are also given for comparison.

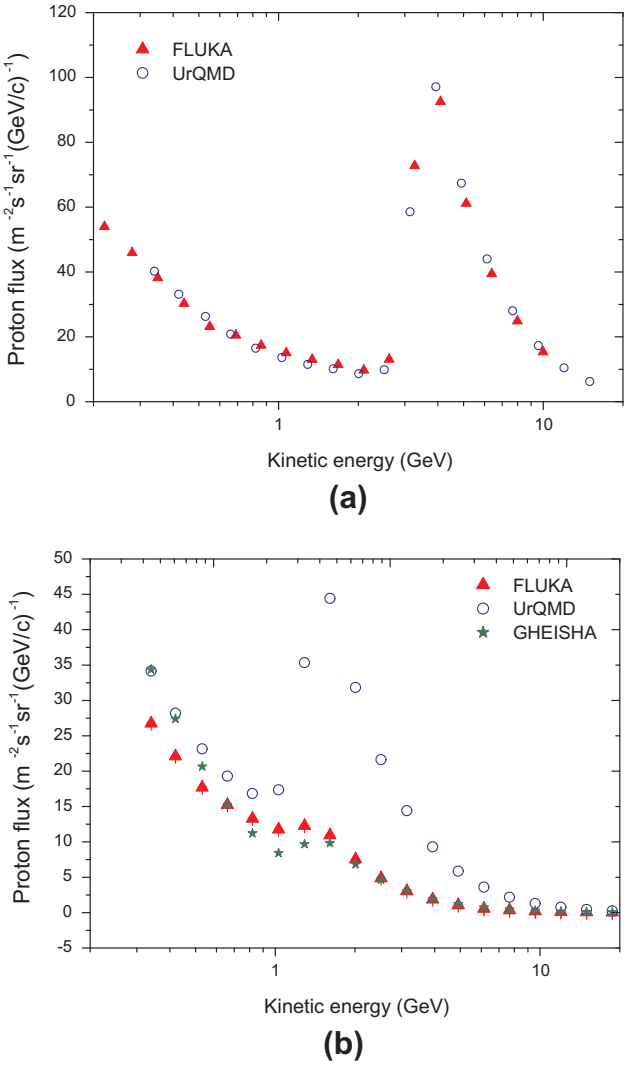

Fig. 3. Contributions from (a) primary protons and (b) primary α particles to the simulated vertical secondary proton flux at an atmospheric depth 10.5 g cm^{-2} at the location of Ft. Sumner. The proton fluxes are generated by using various hadronic interaction models as indicated in the diagram.

displayed in this diagram represents the magnitude of statistical error in the simulations.

At mountain altitude and at the sea-level, the $\bar{p}$ fluxes generated by UrQMD are found to be consistent with the BESS measurements within error bars. Such UrQMD-derived fluxes are, however, higher than the measured values at very high altitude. On the other hand, the FLUKA-generated fluxes are consistently higher than the measured values at all the atmospheric depths. The disagreement between the FLUKA-derived $\bar{p}$ spectra and the BESS observations is maximum at very high altitude and minimum at the sea level.

The results of our simulation for antiproton flux up to about 100 GeV at an atmospheric depth 10.7 g cm^{-2} is displayed in Fig. 5. To minimize statistical fluctuations, 40–50 million events are generated to obtain the flux from each model in this figure. The BESS measurements at Ft. Sumner [84] are also compared in Fig. 5. The fluxes generated by UrQMD + QGSJET and FLUKA + QGSJET combinations are found to differ significantly at the lower energy end; whereas, they predict nearly the same flux at higher (above about 5.0 GeV) energies. As we move to higher energies, the simulated $\bar{p}$ flux is increasingly influenced by the particle interaction characteristics at higher energies. We have, so far, considered just a single model (QGSJET) for describing particle interactions above 80 GeV/n. It is, therefore, expected that the stated combinations of models will give nearly the same flux at such higher energies.

To probe further into the situations at energies ranging roughly from about 10 GeV to 100 GeV, we simulate additional sets of data by replacing QGSJET by VENUS, NEXUS and EPOS interaction models to describe particle interactions above 80 GeV/n, while continuing with FLUKA below 80 GeV/n. The spectra obtained from such combinations are also shown in Fig. 5. In the absence of any experimental data, we could not judge the merit of the VENUS, NEXUS or the EPOS model over the QGSJET model as far as the $\bar{p}$ production in the atmosphere is concerned. It is, however, clear from the comparison of $\bar{p}$ fluxes in Fig. 5 that the theoretically predicted antiproton flux has strong dependence on high energy interaction models over the energy range considered here.

A characteristic feature of the atmospheric antiproton spectrum is that it peaks at around 2 GeV, decreasing rapidly towards lower energies, that is reflected in the simulated spectra as displayed in Fig. 5. Such a feature is not clearly visible in the BESS atmospheric observations because of the limited energy range of the experimental spectra.

To quantify the uncertainties in the theoretical $\bar{p}$ fluxes to a certain extent, we plot the ratios of average $\bar{p}$ fluxes predicted by each

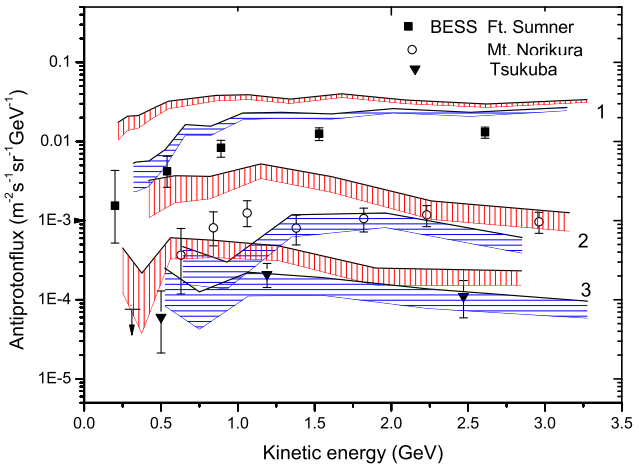

Fig. 4. A diagram depicting the simulated differential spectra of vertical atmospheric antiprotons at multiple atmospheric depths. In this figure, the red (vertically striped) bands and the blue (horizontally striped) bands represent the results simulated with FLUKA and UrQMD models; whereas, the uppermost (marked by the numeral 1), middle (marked by the numeral 2) and the lowermost (marked by the numeral 3) pair of bands represent $\bar{p}$ fluxes at balloon altitude (at the location of Ft. Sumner, USA), at mountain altitude (Mt. Norikura, Japan) and at the sea-level (Tsukuba, Japan) respectively. Corresponding measurements by BESS-2001 [84], BESS-1999 [72] and BESS-1997 [84] experiments are also given for comparison. Note that the bands marked by the numeral 2 are obtained from our previous simulations [24]. (For interpretation of the references to colour in this figure legend, the reader is referred to the web version of this article.)

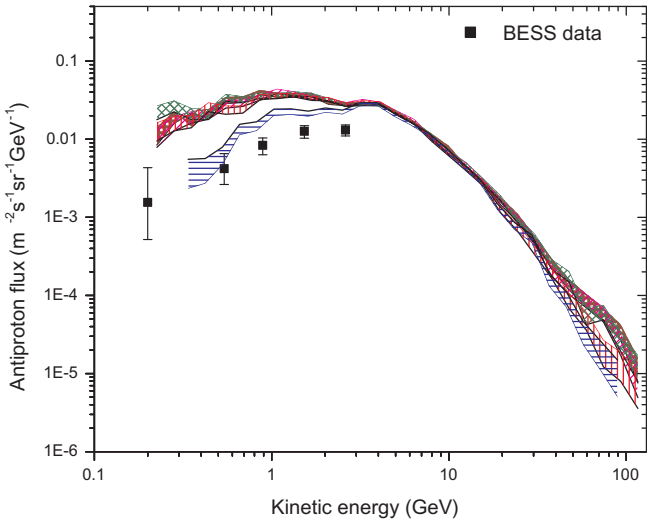

Fig. 5. Atmospheric vertical antiproton flux simulated with UrQMD + QGSJET, FLUKA + QGSJET, FLUKA + VENUS, FLUKA + NEXUS and FLUKA + EPOS models at an atmospheric depth 10.7 g cm^{-2} at the location of Ft. Sumner, USA for the kinetic energy of antiprotons within a range 0.2–100 GeV. Here, the blue (horizontally striped) band depicts the UrQMD + QGSJET combination, the red (vertically striped) band depicts the FLUKA + QGSJET combination, the magenta band (shaded by right-tilted lines) represents the FLUKA + NEXUS combination, the green (cross-hatched) band represents the FLUKA + VENUS combination and the brown (square-hatched) band represents the FLUKA + EPOS combination. Fluxes obtained by the BESS-2001 observation are also given for comparison. (For interpretation of the references to colour in this figure legend, the reader is referred to the web version of this article.)

of the FLUKA + QGSJET, UrQMD + QGSJET, FLUKA + VENUS and the FLUKA + EPOS combinations to the average fluxes obtained from the FLUKA + NEXUS combination (arbitrarily chosen as reference for the comparison) that are displayed in Fig. 6. While such ratios are found to be close to unity in the energy range around 3 – 10 GeV for all the models, they significantly deviate from each

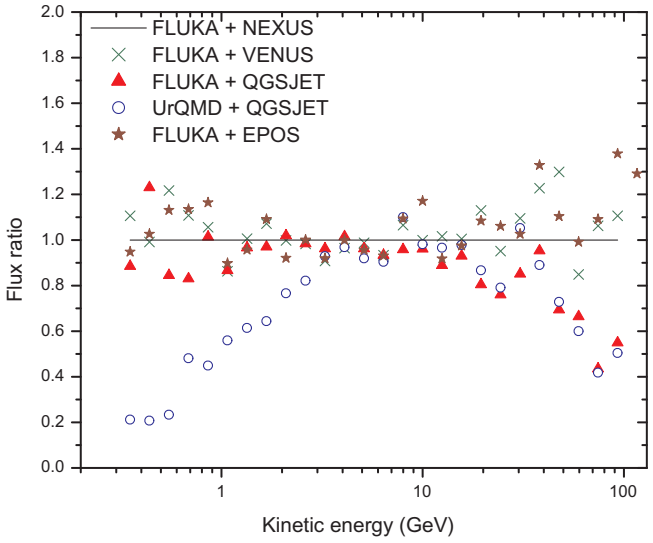

Fig. 6. Ratios of the mean atmospheric antiproton fluxes simulated with each of the FLUKA + QGSJET, FLUKA + VENUS, FLUKA + EPOS and the UrQMD + QGSJET combinations to the ones simulated with the FLUKA + NEXUS model for various values of kinetic energy of the antiprotons at a mean atmospheric depth 10.7 g cm^{-2} at the location of Ft. Sumner, USA.

other at higher energies. The flux-ratios even show more than 60% variation for different models at energies around 100 GeV. In Fig. 6, we find that the QGSJET-predicted mean flux at kinetic energies above about 10 GeV is substantially lower than those predicted by the NEXUS or the VENUS model. The EPOS1.6 model follows a trend similar to that shown by VENUS at such high energies. Below about 3 GeV, the UrQMD model gives appreciably lower fluxes than those obtained by the FLUKA model as was already noted in Fig. 5. Possibilities of statistical fluctuations are, of course, present in such results, but such systematic deviations as depicted in Fig. 6 can not be accommodated in terms of statistical fluctuations.

Since all the interaction models used here are appropriately tuned to the results obtained from the known collider and other experiments, the difference between the predictions of such models are mainly due to our limited understanding of high energy particle interactions.

5. Summary and discussion

Atmospheric proton and antiproton fluxes at different atmospheric levels are calculated in this article by using MC simulations with different particle interaction models and compared to the BESS experimental results. For spectra below about 10 GeV, corresponding to the experimental measurements, only the interaction models FLUKA and UrQMD are relevant. Here, we further extend our study of the atmospheric $\bar{p}$ flux up to 100 GeV where the high energy particle interaction models QGSJET01c, VENUS4.12, NEXUS3.97 and EPOS1.6 start to influence the simulated flux. As a consequence, we can examine the effect of such interaction models on the calculated $\bar{p}$ spectra in this article. The results of such study lead to the following observations.

1. It is interesting to note that the predictions of $\bar{p}$ fluxes obtained from FLUKA and UrQMD show significant deviations from each other, particularly at energies below about 3 GeV.
   The model UrQMD presents reasonable description of the BESS $\bar{p}$ data at mountain altitude and at sea level; whereas, it overestimates the antiproton flux at very high altitude thus possibly indicating that there is an enhanced production of $\bar{p}$ followed

by an enhanced annihilation in this particular model. Such an enhanced production of $\bar{p}$ in UrQMD may not be entirely unexpected as the model yields a higher multiplicity in comparison with the fixed target experiments.

The fact that FLUKA consistently yields a higher $\bar{p}$ flux than the measurements at all the observation levels possibly indicates a strongly enhanced $\bar{p}$ production in this model unless we assume that the BESS experiments have missed a sizable $\bar{p}$ events. The latter possibility is, however, thin as the fluxes obtained from UrQMD is consistent with the measured fluxes at sea-level and at mountain altitude. Atmospheric $\bar{p}$ annihilation also appears to be slightly enhanced in the FLUKA model as the disagreement between the FLUKA-generated $\bar{p}$ spectra and the ones obtained from the BESS measurements is found to decrease with increasing atmospheric depth.

As mentioned in Section 2, FLUKA mainly exploits the DPMJET-III model in describing high energy nucleon-nucleus interactions. DPMJET-III is known to moderately reproduce the energy dependence of antiproton to proton ratio at $y_{cm} = 0$ in proton-proton collisions as measured in the accelerator experiments [27]. It also reproduces the BRAHMS findings (from the RHIC experiment) regarding the dependence of antiproton to proton ratio on cms rapidity practically within experimental errors [22]. Although the consistency of the model parameters can not be checked in the energy range relevant for the present study as there is no direct experimental data on antiproton rapidity distribution in collisions with air or similar targets, the disagreement between the FLUKA-based fluxes and the measured fluxes on such a scale as noticed in the present study is, nevertheless, not an expected one.

It is worthwhile to note that the $\bar{p}$ flux obtained by Stephens [78] through a three dimensional MC simulation within a phenomenological framework was also found to be substantially higher in comparison with the BESS-observed flux at balloon altitude and in comparison with the theoretical unidirectional flux. Stephens [78] ascribed such a discrepancy to the use of the global spectra of primary cosmic ray particles instead of those observed by the BESS experiments. Such a possibility seems to be unlikely as the difference between the measured flux and the theoretically predicted flux is rather large in this particular case. As mentioned earlier, the balloon in the BESS-2001 experiment at Ft. Sumner was initially floated at an atmospheric depth 4.5 g cm^{-2} from where it started to descend slowly to an atmospheric depth of around 30.0 g cm^{-2} before the termination of the experiment [84]. In the absence of any knowledge regarding the effective observation time at each atmospheric depth, the $\bar{p}$ flux at balloon altitude is computed in the present investigation (and in [78]) at 10.7 g cm^{-2} that was the mean atmospheric depth for the BESS-2001 experiment. As the $\bar{p}$ flux in the atmosphere does not vary linearly with the atmospheric depth, such an inability to precisely determine the atmospheric depth could be at least one of the possible reasons for the difference between the simulated and the measured fluxes at the balloon altitude.

We here note that a few phenomenological MC simulations yield $\bar{p}$ fluxes that are consistent with the BESS observation at balloon altitude except below 1.0 GeV unless it is assumed that the tertiary antiprotons do not loose their energy in collisions with atmospheric nuclei [84]. Notwithstanding such assumptions, none of the above simulations consistently describe the BESS measurements of $\bar{p}$ spectra at all the observation levels. The present study, on the other hand, seems to suggest that the BESS observations of $\bar{p}$ spectra are relatively well described by the UrQMD model.

2. The results presented in this article show a significant discrepancy between the BESS-observed secondary proton spectra at very high altitude below the geomagnetic rigidity cutoff and the ones obtained from the interaction models FLUKA and UrQMD, particularly at the low energy part of the observed spectra. It is worth noting here that the re-entrant albedo particles, a consideration of which has been left out of the present investigation, are unlikely to be the cause of such a difference between the measured and the simulated flux of the secondary protons. This is because of the fact that the flux of such re-entrant albedo protons, as measured by the AMS experiment [13], is smaller by more than an order in comparison with the BESS-observed secondary proton flux below the geomagnetic cutoff till down to at least 0.3 GeV. We also note that the BESS collaboration (see the footnote in Ref. [3]) found no such re-entrant albedo proton flux in their observation at the balloon altitude.

   The difference that we find between the simulated and the observed proton spectra at very high altitude is in apparent contradiction with the results of our earlier simulations [24] that display reasonable agreement with the BESS-observed proton flux at mountain altitude. Fig. 2(a) and (b) in Section 4, however, demonstrate that the model-predicted proton fluxes at a lower altitude are indeed closer to the observed proton fluxes in comparison with those at a higher altitude. We may thus infer from the above results that the BESS observations seem to favor a higher production rate of protons in the nucleon-air collisions than the ones implemented in the FLUKA and the UrQMD models. We, however, note that the results of a single experimental measurement may contain uncertainties so that further observations of cosmic ray proton fluxes at multiple altitudes, along with the corresponding MC simulations, may be required to arrive at a definite conclusion on this particular issue.

3. The recent findings of the PAMELA experiment on positron excess [7,8] but no antiproton excess [6] in the energy range from sub-GeV to about 180 GeV lead to a nontrivial constraint on dark-matter models that try to account for the positron excess [31,50,58]. In the stated findings, the excess is determined by comparing with the background predictions from cosmic ray propagation models. The background $\bar{p}$ spectrum, that originates from the hadronic production induced by cosmic rays on the ISM, is generally calculated with the GALPROP numerical propagation code either by applying the parametrization of the invariant $\bar{p}$ production cross section [63] or by implementing the DTUNUC MC code [75]. Uncertainties in $\bar{p}$ flux due to the uncertainties in nuclear parameters, that are estimated from the parametrization of the maxima and the minima of the measured inclusive $\bar{p}$ cross sections in hadron-hadron and hadron-nucleus collisions, were found earlier to be about 22–25% [32]; whereas, the uncertainties in the nuclear parameters of the DTUNUC program, that essentially rests on the DPM model, were estimated to be about 40% [75].

   The present study also indicates, albeit indirectly, that the theoretical galactic $\bar{p}$ spectrum may contain large uncertainties due to the uncertainties in our knowledge of the particle interaction characteristics. Our investigation shows that at energies below about 3 GeV, the BESS observed atmospheric antiproton fluxes, at an atmospheric depth roughly comparable to the depth traversed by the cosmic rays in the Galaxy, are substantially lower than those obtained with the model FLUKA that may be regarded as a DPM class of model. At energies above about 10 GeV, the model predictions cannot be tested experimentally but, importantly, the predictions from different popular microscopic high energy interaction models tend to differ appreciably. In this context, we note that the model EPOS is known to produce more baryons/antibaryons in comparison with most of the other models including QGSJET that seems to be reflected in our results; see Figs. 5 and 6 in Section 4. Our investigation in

Fig. 6, in fact, suggests that the amount of uncertainty between different model predictions is not the same at all energies. Around 300 MeV, such uncertainty is as large as 80% that reduces substantially towards higher energies, particularly above about 3 GeV. Above 10 GeV, the uncertainty, however, increases again with energy and even becomes more than 60% at about 100 GeV. In the near future, we plan to take up a further investigation on the secondary antiproton spectrum by extending the maximum kinetic energy of such antiprotons to about 180 GeV or even beyond and by exploiting the updated versions of high energy interaction models, such as the QGSJET-II [64,65] and the EPOS 1.99 [68] models, in the framework of CORSIKA 6.980 (along with FLUKA 2011.2 to simulate below 80 GeV/n) for a better understanding of the recent PAMELA observations [8]. It may also be important here to note that the proposed measurements of $p + C \to \bar{p}$ and $\pi + C \to \bar{p}$ by the NA61/SHINE fixed-target experiments [5,14] at a few hundred GeV (lab) energy is expected to assist us in improving our understanding on the production of antiprotons thereby resolving the noted discrepancies between the interaction models in near future.

Finally, we may argue that the magnitude of uncertainties quoted in the theoretical calculations of $\bar{p}$ flux, that are obtained by employing semi-phenomenological fit to the experimental data, should perhaps be taken with some caution. This is because of the fact that the errors in the experimental results, based on which the model parameters are fitted or parametrized, are often underestimated or overlooked that may, in turn, affect the entire theoretical prediction. Well known examples are the inelastic $p - \bar{p}$ cross-sections that were measured by three different experiments at FERMILAB and the values at $\sqrt{s} = 1800$ GeV were found to vary from 80.03 ± 2.24 mb to 71.71 ± 2.02 mb [2,12,15]. Therefore, it is obvious that the model parameters that were tuned in accordance with the earlier quoted experimental $p - \bar{p}$ cross-sections would suffer from additional uncertainties. Thus, the consistencies of the predictions of a model in different circumstances may alone provide the validity of its inputs. In view of the results of the present analysis, a detailed study of the galactic $\bar{p}$ flux by exploiting different microscopic interaction models seems to be worth pursuing in the context of the PAMELA observation and its interpretation in terms of the standard/non-standard (dark matter, etc.) sources.

Acknowledgements

A.B. and B.B. acknowledge the support provided by the Department of Science and Technology (DST, Govt. of India) through the Grant No. SR/S2/HEP-14/2007. S.K.G., P.S.J. and S.R. thank the DST (Govt. of India) for support under the IRHPA scheme. We thank two anonymous reviewers for their constructive criticisms on an earlier version of the manuscript that has helped us to improve the quality of this version. We also thank Dr. R. Engel and Dr. T. Pierog for helping us with certain aspects of the CORSIKA code.

References

[1] T. Abbott et al., Phys. Rev. C 47 (1993) R1351.
[2] F. Abe et al., Phys. Rev. D 50 (1994) 5550.
[3] K. Abe et al., Phys. Lett. B 564 (2003) 8.
[4] K. Abe et al., Phys. Lett. B 645 (2007) 472.
[5] N. Abgrall et al., CERN-SPSC-2008-018, 2008.
[6] O. Adriani et al., Phys. Rev. Lett. 102 (2009) 051101.
[7] O. Adriani et al., Nature 458 (2009) 607.
[8] O. Adriani et al., Phys. Rev. Lett. 105 (2010) 121101.
[9] C.W. Akerlof et al., Phys. Rev. D 3 (1971) 645.
[10] J. Alcaraz et al., Phys. Lett. B 472 (2000) 215.
[11] J. Alcaraz et al., Phys. Lett. B 494 (2000) 193.
[12] N.A. Amos et al., Phys. Rev. Lett. 68 (1992) 2433.
[13] M. Aguilar et al., Phys. Rep. 366 (2002) 331.
[14] N. Antoniou et al., CERN-SPSC-2007-004, 2007; CERN-SPSC-2007-019, 2007.
[15] C. Avila et al., Phys. Lett. B 445 (1999) 419.
[16] M. Baker, K.A. Ter-Martirosyan, Phys. Rep. 28 (1976) 1.
[17] H.B. Barber et al., Phys. Rev. D 22 (1980) 2667.
[18] B. Baret, L. Derome, C.-Y. Huang, M. Buénerd, Phys. Rev. D 68 (2003) 053009.
[19] D.S. Barton et al., Phys. Rev. D 27 (1983) 2580.
[20] S.A. Bass et al., Prog. Part. Nucl. Phys. 41 (1998) 225.
[21] G. Battistoni, S. Muraro, P.R. Sala, F. Cerutti, A. Ferrari, S. Roesler, A. Fassò, J. Ranft, in: M. Albrow, R. Raja (Eds.), Proceedings of the Hadronic Shower Simulation Workshop, Fermilab 6–8 September 2006, AIP Conference Proceeding, vol. 896, 2007, p. 31.
[22] I.G. Bearden et al., Phys. Lett. B 607 (2005) 42.
[23] G. Bertone, D. Hooper, J. Silk, Phys. Rep. 405 (2005) 279.
[24] A. Bhadra, S.K. Ghosh, P.S. Joarder, A. Mukherjee, S. Raha, Phys. Rev. D 79 (2009) 114027.
[25] M. Bleicher et al., J. Phys. G 25 (1999) 1859.
[26] M. Bleicher, A. Keränen, J. Aichelin, S.A. Bass, F. Becattini, K. Redlich, K. Werner, Phys. Rev. Lett. 88 (2002) 20251.
[27] F.W. Bopp, J. Ranft, R. Engel, S. Roesler, Phys. Rev. C 77 (2008) 014904.
[28] T. Bowen, A. Moats, Phys. Rev. D 33 (1986) 651.
[29] A. Capella, U. Sukhatme, C.-I. Tan, J. Tran Thanh van, Phys. Rep. 236 (1994) 225.
[30] P. Capiluppi et al., Nucl. Phys. B 79 (1974) 189.
[31] M. Cirelli, M. Kadastik, M. Raidal, A. Strumia, Nucl. Phys. B 813 (2009) 1.
[32] F. Donato et al., Astrophys. J. 563 (2001) 172.
[33] H.J. Drescher, M. Hladk, S. Ostaptchenko, T. Pierog, K. Werner, Phys. Rep. 350 (2001) 93.
[34] H.J. Drescher, M. Bleicher, S. Soff, H. Stöcker, Astropart. Phys. 21 (2004) 87.
[35] R.P. Duperray, C.-Y. Huang, K.V. Protasov, M. Buénerd, Phys. Rev. D 68 (2003) 094017.
[36] R.P. Duperray et al., Phys. Rev. D 71 (2005) 083013.
[37] A. Fassò, A. Ferrari, J. Ranft, P.R. Sala, in: Proceedings of the Specialists Meeting on Shielding Aspects of Accelerators, Targets and Irradiation Facilities (Arlington, USA) (OECD/NEA, 1994), p. 287.
[38] A. Ferrari, P.R. Sala, in: Proceedings of the 1993 Conference on Monte Carlo Simulation in High Energy and Nuclear Phys. (Tallahassee, USA), World Scientific, Singapore, 1994, p. 277.
[39] A. Ferrari, P.R. Sala, A. Fassò, J. Ranft, Report CERN-2005-10 (2005), INFN-TC_05/11, SLAC-R-773 (2005).
[40] H. Fesefeldt, RWTH Aachen Report No. PITHA-85/02, 1985.
[41] T.K. Gaisser, M. Honda, P. Lipari, T. Stanev, in: Proceedings of the 27th International Cosmic Ray Conference, Hamburg, Germany, vol. 5, 2001, p. 1643.
[42] L.G. Gleeson, W.I. Axford, Astrophys. J. 154 (2004) 1011.
[43] V.N. Gribov, Sov. Phys. JETP 26 (1968) 414.
[44] V.N. Gribov, Sov. Phys. JETP 29 (1969) 483.
[45] V.N. Gribov, Sov. Phys. JETP 30 (1970) 709.
[46] S. Haino et al., Phys. Lett. B 594 (2004) 35.
[47] S.W. Hawking, Nature (London) 248 (1974) 30.
[48] D. Heck, J. Knapp, J.N. Capdevielle, G. Schatz, T. Thouw, Forschungszentrum Karlsruhe Report No. FZKA 6019, 1998.
[49] D. Heck, Nucl. Phys. B, Proc. Suppl. 151 (2006) 127.
[50] D. Hooper, A. Stebbins, K.M. Zurek, Phys. Rev. D 79 (2009) 103513.
[51] C.-Y. Huang, L. Derome, M. Buénerd, Phys. Rev. D 68 (2003) 053008.
[52] J.R. Johnson et al., Phys. Rev. D 17 (1978) 1292.
[53] G. Jungman, M. Kamionkowski, K. Griest, Phys. Rep. 267 (1996) 195.
[54] A.B. Kaidalov, Surv. High Energy Phys. 13 (1999) 265.
[55] N.N. Kalmykov, S.S. Ostapchenko, A.I. Pavlov, Nucl. Phys. B, Proc. Suppl. 52 (1997) 17.
[56] M. Kamionkowski, M.S. Turner, Phys. Rev. D 43 (1991) 1774.
[57] P. Kiraly, J. Szabelski, J. Wdowczyk, A.W. Wolfendale, Nature (London) 293 (1981) 120.
[58] M. Lattanzi, J.I. Silk, Phys. Rev. D 79 (2009) 083523.
[59] J. Linsley, private communication.
[60] F.M. Liu, J. Aichelin, M. Bleicher, H.J. Drescher, S. Ostapchenko, T. Pierog, K. Werner, Phys. Rev. D 67 (2003) 034011.
[61] K.G. McCracken, F.B. McDonald, J. Beer, G. Raisbeck, F. Yiou, J. Geophys. Res. 109 (2004) A12103.
[62] J.W. Mitchell et al., Phys. Rev. Lett. 76 (1996) 3057.
[63] I.V. Moskalenko, A.W. Strong, J.F. Ormes, M.S. Potgieter, Astrophys. J. 565 (2002) 280.
[64] S.S. Ostapchenko, Nucl. Phys. B (Proc. Suppl.) 151 (2006) 143–147.
[65] S.S. Ostapchenko, Phys. Rev. D 74 (2006) 014026.
[66] V.S. Ptuskin, I.V. Moskalenko, F.C. Jones, A.W. Strong, V.N. Zirakashvili, Astrophys. J. 642 (2006) 902.
[67] T. Pierog, H.J. Drescher, F. Liu, S. Ostapchenko, K. Werner, Nucl. Phys. A 715 (2003) 895c.
[68] T. Pierog, K. Werner, Nucl. Phys. Proc. Suppl. 196 (2009) 102–105.
[69] S. Roesler, R. Engel, J. Ranft, in: Proceedings of the Monte Carlo 2000 Conference (Lisbon), Springer, Berlin, 2001, p. 1033. Available from: <hep-ph/0012252>.
[70] T.J. Sabaka, R.A. Langel, J.A. Conrad, J. Geomag. Geoelect. 49 (1997) 157.
[71] T. Sanuki et al., Astrophys. J. 545 (2000) 1135.

[72] T. Sanuki et al., Phys. Lett. B 577 (2003) 10.
[73] T. Sanuki, M. Honda, T. Kajita, K. Kasahara, S. Midorikawa, Phys. Rev. D 75 (2007) 043005.
[74] M.A. Shea, D.F. Smart, J. Geophys. Res. 72 (1967) 2021.
[75] M. Simon, A. Molnar, S. Roesler, Astrophys. J. 499 (1998) 250.
[76] S.A. Stephens, Astrophys. Space Sci. 76 (1981) 87.
[77] S.A. Stephens, Astropart. Phys. 6 (1997) 229.
[78] S.A. Stephens, Adv. Space Res. 35 (2005) 142.
[79] Y. Sugaya et al., Nucl. Phys. A 634 (1998) 115.
[80] I.G. Usoskin, A.-H. Katja, G.A. Kovaltsov, K. Mursula, J. Geophys. Res. 110 (2005) A12108.
[81] B. Weibel-Sooth, P.L. Biermann, H. Mayer, Astron. Astrophys. 330 (1998) 389.
[82] K. Werner, Phys. Rep. 232 (1993) 87.
[83] K. Werner, F.M. Liu, T. Pierog, Phys. Rev. C 74 (2006) 044902.
[84] K. Yamato et al., Phys. Lett. B 632 (2006) 475.

The knee in the cosmic ray energy spectrum from the simutaneous EAS charged particles and muon density spectra

Biplab Bijay[1,a], Prabir Banik[1,b] and Arunava Bhadra[1,c]
[1] *High Energy & Cosmic Ray Research Centre, University of North Bengal, Siliguri, West Bengal, India 734013*
[a] *biplabbijay@rediffmail.com,*
[b] *pbanik74@yahoo.com*
[b] *aru_bhadra@yahoo.com*

In this work we examine with help of Monte Carlo simulation whether a consistent primary energy spectrum of cosmic rays emerges from both the experimentally observed total charged particles and muon size spectra of cosmic ray extensive air showers considering primary composition may or may not change beyond the knee of the energy spectrum.

I. INTRODUCTION

The primary energy spectrum of all particle cosmic rays is known to exhibit a power law behavior with few features including a slight bend of the spectrum at about 3 PeV, the so called knee of the spectrum, where the power law spectral index changes from about -2.7 to nearly -3.0. The knee is generally believed to be of astrophysical origin. The common explanations of the knee include rigidity-dependent upper limit on the energy that cosmic ray protons can attain at supernova remnants [1], leakage of cosmic rays from the galaxy [2], a nearby single source [3], mass distribution of progenitors of cosmic ray sources [4] etc.

The primary cosmic ray particles after entering into the Earth's atmosphere interact with the atmospheric nuclei and produce secondary particles. The detection of cosmic rays above the atmosphere is thus the only way to obtain direct measurements of the characteristics of primary cosmic ray particles including their energy spectra and mass composition. The energy spectrum of primary cosmic rays has been measured directly through satellite or balloon borne detectors up to few hundreds TeV. Above such energy direct methods for studying primary cosmic rays become inefficient due to sharp decrease in the flux of primary particles and the study of primary cosmic rays has to perform indirectly, through the observation of cosmic ray extensive air shower (EAS) which are cascades of secondary particles produced by interactions of cosmic ray particles with atmospheric nuclei. From their experimental results the Moscow State University group first noticed that the EAS electron size (total electron content) spectrum had a pronounced increase of slope (β increases suddenly) at a size corresponding to a primary energy of about 3 PeV [5] which was inferred as due to a break or the knee in the cosmic ray primary energy spectrum. Since then many EAS experiments covering this energy range confirm such a break in the spectral index of electron size spectrum and the existence of the knee in the cosmic ray energy spectrum is now considered as a well- established fact.

Some authors, however, cast doubt on the astrophysical origin of the knee. In particular a new type of interaction that transfers energy to a not yet observed component with interaction threshold in the knee region was proposed as the cause of the observed knee feature in the shower size spectrum [6, 7]. However, such a proposal has not received any support from the LHC experiment against the expectations. On the other hand Stenkin [8, 9] refuted the reality of the knee in the primary cosmic ray energy spectrum on the ground that the knee has been noticed observationally only in the electromagnetic component of EAS but not in the muonic and the hadronic components of EAS. In other words the knee feature in the primary cosmic ray energy spectrum is not consistently revealed from electromagnetic, muonic and hadronic components of EAS. Stenkin proposed an alternative explanation of the break in shower size spectrum in terms of coreless EAS [8, 9]. Further a new experiment PRISMA has been proposed to investigate the situation [10].

While arguing against the astrophysical knee, Stenkin did not consider any change in primary mass composition in the knee region on air shower muon and electron spectra [8]. Here it is worthwhile to mention that the almost all the well known models of the knee generally predict for a change in the mass composition of cosmic rays across the knee energy. For instances, the scenarios like rigidity dependent acceleration mechanism in the source or leakage from the Galaxy (which is also a rigidity dependent effect) predict for a heavier cosmic ray mass composition beyond the knee while the models based on nuclear photo-disintegration processes in the presence of a background of optical and soft UV photons in the source region predict for a lighter composition above the knee. The modern precise EAS experiments estimated primary energy spectra of different mass groups or even of various elements based on the deconvolution of either measured electron size distribution along with the information of muon content (as a function of electron size) or from a measured two-dimensional electron muon number distribution. Though conclusions of different experiments on primary mass composition in the knee region are not unequivocal, majority conclude that the knee represents the

energy at which proton component exhibits cut-off [4] i.e. the knee of the spectrum has been ascribed as the proton knee.

It is thus imperative to examine whether the primary knee feature is consistently revealed in electron and muon components of EAS when primary composition changes from lighter primaries to heavier primaries beyond the knee energy. This is precisely the objective of the present work. Our main emphasis will be to check whether the different EAS observables suggest for consistent spectral indices in the primary cosmic ray energy spectrum before and after the knee considering the fact that primary composition may or may not change across the knee. For this purpose we shall perform a detailed Monte Carlo simulation study of EAS using CORSIKA [11] in the concerned energy range and we will analyze different experimental data on size spectrum of various EAS observables to check the inner consistency. We will also estimate the spectral indices of electron and muon size spectra for different primary composition scenario assuming primary cosmic ray energy spectrum has a knee. The hadronic component is not considered in this work as only few data in this regard are available and more importantly the uncertainties are quite large.

The organization of the paper is as follows. In the next section the principle of deriving the cosmic ray energy spectrum from the EAS observables is outlined briefly in the framework of Bhabha-Heitler theory of electromagnetic cascade . In section III we describe our analysis of cosmic rsy EAS size spectra based on the Monte Carlo simulation study. The procedure adapted for the Monte Carlo simulation of cosmic ray EAS is discussed in the subsection III-A. In the subsection III-B we evaluate spectral index of primary energy spectrum from the measured electron and muon size spectra for different primary composition scenario. The expected shower size and muon size spectra for different mass composition scenario assuming the primary energy spectrum has a knee are obtained in the subsection III-C. Finally we discuss the findings and their probable explanations in the section IV.

II. PRIMARY ENERGY SPECTRUM FROM EAS OBSERVATIONS AND THE KNEE

Usually, cosmic ray EAS arrays employ scintillation detectors for detection of electrons, which is the dominating component among the charged particles in EAS. However, such detectors also detect other charged particles including muons. So essentially EAS observations give information about total charged particle spectrum instead of electron size spectrum . The observational charged particle size (often known as shower size) spectrum in EAS is found to exhibit power law behavior i.e.

$$\frac{dN}{dN_{ch}} \propto N_{ch}^{-\beta_{ch}} \tag{1}$$

Though the development of EAS is a very complicated process that can be properly addressed only via Monte Carlo simulation technique but an idea of how electron and other secondary particle sizes are related to primary energy can be obtained based on the Bhabha - Heitler analytical approach of electromagnetic cascade [12, 13]. A cosmic ray particle interacts with the atmospheric nuclei while moving through the atmosphere and produced dominantly charged and neutral pions. There will be also secondary hadrons (leading particles). Neutral pions quickly decay to photons which subsequently initiate electromagnetic cascades. The charged pions may interact with atmospheric nuclei (thereby further produce secondary particles) or decay depending on their energy. The decay of charged pions yields muons and neutrinos. The energy dependence of total number electrons, muons and hadrons at shower maximum (at which the number of particles in a shower reaches its maximum) in EAS initiated by a nucleus with atomic mass number A and energy E_o can be expressed as [12, 13]

$$N_i^{max} = N_i^o E_o^{\alpha_i} \tag{2}$$

where i stands for e (electron), μ (muon) and h (hadron). For pure electromagnetic cascade and under few simple approximations such as the all electrons have the same energy E_e^c (which is the critical energy (85 MeV in air), at which ionization losses and radiative losses are equal) α_e is nearly equal to 1. Similarly when all muons are considered to have the same energy E_π^c (which is the energy at which the probability for a charged pion to decay and to interact are equal) and taking the charged pion production multiplicity is 10 (constant) $\alpha_\mu \sim 0.85$ [13]. When the effect of inelasticity is taken into consideration, α_μ will be slightly higher, ~ 0.90 [13]. If one considers that total primary cosmic ray energy is distributed between electron and muon component, α_e will be slightly higher, about 1.05 [13].

Two important points to be noted are (i) the total number of electrons increases with energy slightly faster than exactly linear whereas the total number of muons grows with energy slightly less than exactly linear. (ii) The electron number decreases with increasing mass number whereas muon number grows with mass number.

After shower maximum, electron (and hadron) size decreases due to attenuation whereas muon size almost remain constant because of its large attenuation length. Hence at a observational level well passed the shower maximum, the equation (2) is not strictly valid, particularly for electrons and hadrons.

Considering that the electron size spectrum and total charged particle size spectrum are more or less the same, from equations (1) and (2) one can infer the primary cosmic ray spectrum as follows

$$\frac{dN}{dE_o} = \frac{dN}{dN_e^{max}} \frac{dN_e^{max}}{dE_o} \propto E_o^{-\gamma} \tag{3}$$

where

$$\gamma \equiv 1 + \alpha_e(\beta_e - 1) \quad (4)$$

will be the slope of primary cosmic ray differential energy spectrum. Since a sudden change in β_e at a size corresponding to a primary energy of about 3 PeV is observed, consequently a change in γ at 3 PeV is inferred which is the so called knee of the cosmic ray energy spectrum.

Equations (2) and (3) imply that muon and hadron size spectra also should exhibit power law behavior with $\beta_i = 1 + (\gamma - 1)/\alpha_i$. Since $\alpha_\mu < \alpha_e$, change in β_μ should be larger than β_e for a change in γ. Observationally, however, no significant change in β_μ is found. This is why Stenkin objected against the existence of a knee in the primary energy spectrum [8, 9].

Note that the semi-analytical expressions described above, though match reasonably well with the simulation results, are approximated description of cosmic ray cascade in the atmosphere. Moreover, the relation between electron size and energy (Eq. 3) is valid only at shower maximum. So a detailed Monte Carlo simulation study needs to be done to draw any concrete conclusion in this regard.

III. MONTE CARLO SIMULATION STUDY OF SIZE SPECTRUM

In the present work we have simulated EAS for three different mass composition scenario: proton as primary over the whole energy range, secondly proton and Fe respectively as primary below and above the knee energy and finaly Fe as primary over the whole energy range. Subsequently we explore whether a consistent mass composition scenario evolve from simultaneous study of electron and muon size spectra in the knee region. We evaluate α_i from simulation data for proton and iron primaries both below and above the knee and using the observed β_i from experiments, we subsequently estimate γ following the equation () and check whether electron, muon and hadron observations give a consistent primary energy spectrum when primary composition is allowed to change across the knee.

A. Simulation procedure adopted

The air shower simulation program CORSIKA (COsmic Ray SImulation for KAscade) (version 6.690) [11] is employed here for generating EAS events. The high energy (above 80GeV/n) hadronic interaction model QGSJET 01 (version 1c) [14] has been used in combination with the low energy (below 80GeV/n) hadronic interaction model UrQMD [15]. A relatively smaller sample has also been generated using the high-energy interaction model EPOS (version 2.1) [16] and low energy interaction model GHEISHA (version 2002d) [17] to judge the influence of the hadronic interaction models on the results. Note that GHEISHA exhibits a few shortcomings [18, 19] but the low energy interaction models has no significant effect on the total number of secondary particles for primaries in the PeV energy range.

The US-standard atmospheric model with planar approximation which works only for the zenith angle of the primary particles being less than 70^o is adopted. The EAS events have been generated for proton and iron nuclei as primaries at several fixed energy points spreaded between 3×10^{14} to 3×10^{16} eV as well as over a continuous energy spectrum between 3×10^{14} to 3×10^{16} eV with differential energy spectrum slop -2.7and -3.1 below and above the knee (3×10^{15} eV) respectively. The EAS events have been simulated at geographical positions correspond to experimental sites of KASCADE [20] and EAS-TOP [21]. The magnetic fields, observation levels, threshold energies of particle detection and zenith angles are provided accordingly.

B. Inferring Primary cosmic ray spectrum from measured EAS size spectra

Only a few EAS experiments so far measured both β_{ch} and β_μ before and after the knee. Here we would consider the results of two experiments, the KASCADE [22, 23] and EAS-TOP [24]. The KASCADE experiment was considered as one of the most precise air shower experiments in the world which was situated in the site of Forschungszentrum Karlsruhe (Germeny) at an altitude 110 m above sea level at 49.1^o N, 8.4^o E, covering an energy range from about 100 TeV to nearly 100 PeV and was in operation during October 1996 to 2003. The experiment consisted an array of electron and muon detectors, spread over 700 m^2 $\times$ 700 m^2, a central hadron calorimeter with substantial muon detection areas and a tunnel with streamer tube muon telescopes. This multidetector system was used for the study of electromagnetic, muonic and hadronic components of EAS. The experiment was later extended to KASCADE-Grande in 2003 to study primary cosmic rays at higher energies. On the other hand the EAS-TOP array was located at Campo Imperatore, National Gran Sasso Laboratories in Italy, 2005 m a.s.l.,(820 $g\ cm^2$) atmospheric depth. This multi-component experiment consisted of detectors of the electromagnetic, muon, hadron and atmospheric Cherenkov light components for the study of EAS over the energy range 100 TeV to about 10 PeV. Two layers of streamer tubes with total surface area $12 \times 12\ m^2$ was used for detection of EAS muons having threshold energy of 1 GeV.

The results of these two experiments on β_{ch} and β_μ are shown in Table 1. Note that the shower size (N_e) and muon size are generally evaluated from the experimental measured particle (electron/muon) densities by fitting with the lateral density distribution function. To minimize the bias by the functional form of the muon

lateral distribution function, KASCADE experiment introduced the quantity truncated muon number which is essentially the muon size within 40 m and 200 m core distance.

Using the public data of KASCADE experiment provided through KCDC [25] we also estimated β. For vertical air showers ($\theta < 18^o$), we find β equals to 2.54 ± 0.06 and 2.97 ± 0.05 below and above the knee are respectively for total charged particles and 2.96 ± 0.08 and 3.24 ± 0.06 for muons below and above the knee respectively which are closed to KASCADE reported β for vertical showers.

Our target is now to evaluate γ both below and above the knee from the measured β_{ch} and β_{μ} considering the results of KASCADE and EAS-TOP, using the expression (). To estimate α we exploit Monte Carlo simulation method.

The figure 1(a) displays the variation of total charged particle number in EAS obtained with Monte Carlo simulation as a function of energy at KASCADE location for proton primary whereas the variation of muon content with primary energy in proton induced EAS is shown in figure 1(b). Power law fits to the data points are also shown in both the figures. We find that the dependence of shower size on primary energy can be described by a power law with constant spectral index. We have also checked whether the data suggest different spectral slops at lower and higher energies by fitting the data below and above the knee separately. But the so fitted slops are found only to differ within the error limits of the single constant spectral index. The estimated power law indices (α_e and α_{μ}) are displayed in table 1 for proton primary. In figure 2 we have plotted the electron and muon sizes in Fe initiated EAS as a function of primary energy. α_e and α_{μ} for Fe primary are also evaluated from power law fitting and are shown in table 2.

Since β_is are known from observations, we have estimated γ straightway using the expression (). We considered both proton and Fe as primaries below the knee as well as above the knee and evaluated γ. Subsequently we computed $\delta\gamma$ across the knee. The results are given in Table 1 for the KASCADE measurements. It is noticed that no consistent γs below and above the knee emerge from the KASCADE measured electron and muon spectra irrespective of the primary composition. The $\delta\gamma$s from the observed electron and muon spectra also differ significantly.

Results of a similar analysis for the EAS-TOP electron and muon spectra are displayed in figures 3 nad 4 from simulation data and in Table 2. In EAS-TOP location the α of charged particles for proton primary is found quite small than that for the KASCADE location which suggests that α changes with atmospheric depth and close to one at shower maximum. For Fe primary, however, no significant difference in α of charged particles noticed in two stated locations which is probably due to the fact that air showers reaches to its maximum development much earlier for heavier primaries. So even at EAS-TOP location, PeV energy Fe initiated showers are quite old. The spectral index (of primary cosmic ray energy spectrum) derived separately from the EAS-TOP observed electron and muon size spectra is found somewhat mutually consistent when cosmic ray primary is dominantly Fe, both before and after the knee. The $\delta\gamma$s from the observed electron and muon spectra also found mutually consistent for unchanging Fe dominated primary.

C. Electron and muon spectra for astrophysical knee

It appears that the main difficulty of arriving a consistent knee from simultaneous charged particles and muon spectra in EAS as observed by KASCADE experiment is the very small spectral slope difference in muon spectrum across the knee relative to the spectral slope difference in charged particle spectrum. However, such an inference is based on the equation () that follows from consideration of the cascade theory which is an approximate description of complex EAS phenomenology. Here we shall estimate the expected spectral slopes in electron and muon spectra for different primary composition scenario assuming that the primary energy spectrum has a knee. The spectral index of the primary energy spectrum below the energy 3 PeV is taken as -2.7 whereas above 3 PeV it is assumed as -3.1. The EAS are generated from the minimum energy of 100 TeV and only vertical showers are generated.

The electron and muon size spectra at KASCADE location from the simulation results are displayed in figures 5. We considered a change in mass composition after the knee from pure proton to pure iron as well as for unchanged (proton and Fe) mass composition. The knee structure is found present in both electron and muon size spectra for all the mass composition scenario considered. The β value obtained from the simulation results are displayed in Table 4 for the different composition scenario. To identify the position of the knee and also to estimate the β values in electron and muon size spectra we multiply the differential total charged particle (muon) numbers by some suitable power (selected by varying the power index slowly) of total charges particles (muons) to emphasize the small difference in slop and plot it against the total charged particles (muons) in log-log scale. It is found that the points below and above a certain total charged particle number have distinct slops. The best fitted slops give the β below and above the size knee whereas the crossing point of the two straight lines (in log-log scale) give the position of the knee in size spectra.

The spectral index of total charged particle spectrum above the knee obtained from the simulation results is found slightly lower than the observational result whereas for muon spectrum the spectral index below the knee from the simulation data is found slightly larger than the observations. It is also noticed that the spectral index below (or above) the knee depends not only primary composition below (above) the knee of the

TABLE I: The measured spectral indices of primary energy spectrum below and above the knee from the electron and the muon size spectra of KASCADE and EAS-TOP observations

Experiment	Component	$\beta_{<knee}$	$\beta_{>knee}$
KASCADE	electron	2.45 ± 0.06	2.94 ± 0.12
KASCADE	muon (> 490 MeV)	3.05 ± 0.006	3.27 ± 0.01
EAS-TOP	electron	2.61 ± 0.01	3.01 ± 0.06
EAS-TOP	muon (> 1 GeV)	3.12 ± 0.03	3.67 ± 0.07

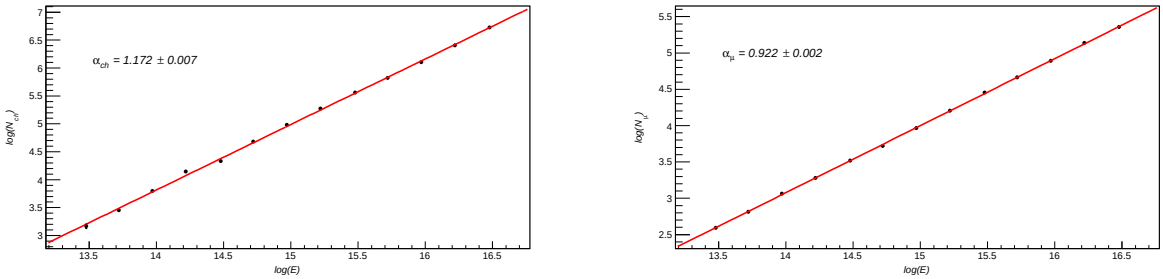

FIG. 1: (Color online) Energy dependence of (a) total charged particles and (b) muon content in proton induced EAS at KASCADE location from the Monte Carlo simulation data.

primary energy spectrum but also the composition above (below) the knee of the energy spectrum, particularly when points close to the knee in the size spectra are considered to determine the spectral index. There are few other important points have been noted:

i) the position of the knee in the charged particles and muon spectra also influence by the primary composition both below and above the knee of the cosmic ray energy spectrum,

ii) the knee in the muon spectrum is slightly more revealing in comparison to that in the electron spectrum for pure proton or Fe primaries over the entire energy range but the same may not be true when primary composition changes across the knee,

and iii) for proton primary before the knee and Fe primary after the knee the muon spectrum exhibits a break not only in the spectral index but also in the flux. The later feature is due to larger muon size in Fe initiated EAS in comparison to proton induced EAS.

A two dimensional plot of electron and muon size spectra for different composition scenario are also obtained and depicted in figures 6 for KASCADE location. An interesting observation is that the knee is not clearly revealed from the two-dimensional plots. Since Fe induced EAS contains lower electrons and higher muons in compare to proton induced EAS, the two dimensional figure exhibits some mismatch in shower and muon sizes around the knee for a sharp change in composition from proton to Fe across the knee which is not observed experimentally.

IV. DISCUSSION AND CONCLUSION

The knee of the primary energy spectrum has long been inferred from the break in shower size spectrum of cosmic ray EAS at certain shower size corresponding to few PeV primary energy. Few authors, particularly Stenkin, however, objected the existence of the knee in the primary energy spectrum noting that the muon size spectrum of cosmic ray EAS does not show any prominent break against the expectations based on cascade theory.

It is found from the present analysis that when a hybrid approach is employed involving cascade theory (to have a relation between the spectral index of primary energy spectrum and the spectral indices of EAS electron and muon size spectra) and the Monte Carlo simulation (invoked to get the relation between electron and muon sizes with primary energy) the EAS-TOP observations on total charged particle and muon spectra consistently infer a knee in the primary energy spectrum provided the primary is pure unchanging iron whereas no consistent primary spectrum emerges from simultaneous use of the KASCADE observed total charged particle and muon spectra.

When a pure Monte Carlo approach is adopted to examine the expected size spectra for a given primary energy spectrum with different mass composition, it is found that for pure unchanging proton or Fe primaries the difference in spectral slops below and above the knee of the size spectrum is larger for muon spectrum than the electron spectrum. However, when mass composition changes across the knee the situation becomes quite complex. In such a situation estimating β properly is challenging, particularly for total charged particle spec-

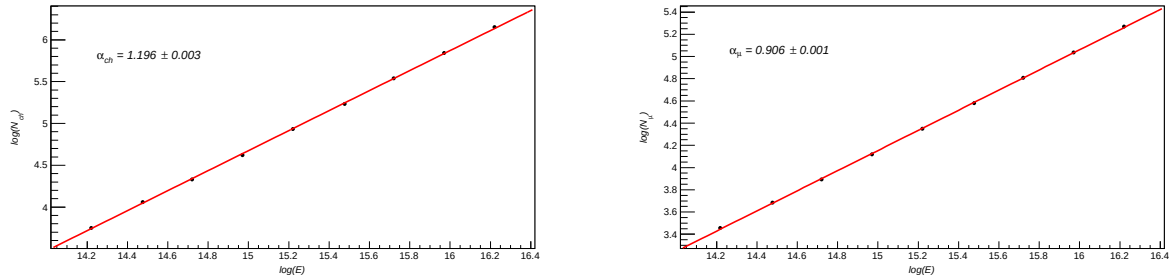

FIG. 2: (Color online) Same as Figure 1 but in Fe initiated EAS.

TABLE II: Spectral indices of primary energy spectrum below and above the knee from the electron and the muon size spectra of KASCADE observations

Primary before the knee	Primary after the knee	Secondary	$\alpha_{<knee}$	$\alpha_{>knee}$	$\gamma_{<knee}$	$\gamma_{>knee}$	$\Delta\gamma$
Proton	Proton	electron	1.172 ± 0.007	1.172 ± 0.007	2.70 ± 0.08	3.27 ± 0.16	0.57 ± 0.24
		Muon (> 490 MeV)	0.922 ± 0.002	0.922 ± 0.002	2.89 ± 0.01	3.09 ± 0.02	0.20 ± 0.04
Proton	Fe	electron	1.172 ± 0.007	1.196 ± 0.003	2.70 ± 0.08	3.32 ± 0.14	0.62 ± 0.22
		Muon (> 490 MeV)	0.922 ± 0.002	0.906 ± 0.001	2.89 ± 0.01	3.05 ± 0.02	0.16 ± 0.03
Fe	Fe	electron	1.196 ± 0.003	1.196 ± 0.003	2.73 ± 0.08	3.32 ± 0.14	0.59 ± 0.22
		Muon (> 490 MeV)	0.906 ± 0.001	0.906 ± 0.001	2.86 ± 0.01	3.05 ± 0.02	0.19 ± 0.03

trum; the β value and the position of the knee depend on primary composition both below and above the knee of the primary energy spectrum and the points close to the knee in the size spectra may change the overall slope considerably. For instance in the simple situation where proton and Fe are the dominating component below and above the knee of the primary energy spectrum, the contribution of Fe, which gives a comparative lower total number of charged particles, leads to a flatter shower size spectrum below the knee, unless the points closed to the knee in the size spectrum are totally ignored to evaluate the slopes. On the other hand Fe induced EAS contains comparatively larger muon number. Hence the slopes of the muon size spectrum does not alter much for the stated changing composition scenario but there will be a mismatch in the flux at the knee of the muon size spectrum. Non observation of any break in flux level at the knee position of the muon size spectrum in any experiment suggests that there is no abrupt change in primary composition across the knee; the composition either changes slowly above the knee or it changes from a lighter dominating mixed composition to heavier dominated mixed composition without appreciable change in average primary mass. In such changing mass composition scenario, the break in EAS muon size spectrum may not be more revealing than that in total charged particle spectrum against the common perception.

We thus conclude that though the derivation of the size spectrum from observed data looks to be rather straight forward process, but in practice it is a quite complex issue particularly owing to the uncertainty in primary mass composition. The simultaneous use of the measured EAS total charged particle and muon size spectra to infer the primary energy spectrum is certainly a better approach but it requires a careful and experiment specific analysis. The two-dimensional differential spectrum contents substantially higher information than those of two one-dimensional ones and hence used to infer primary spectrum and composition but one dimensional spectra also carry important and exclusive signatures about primary energy spectrum and composition which may be accommodated to get more reliable estimates about cosmic ray primaries.

[1] C. E. Fichtel, and J. Linsley, Astrophys. J. **300**, 474 (1986)
[2] V. L. Ginzburg, and S. I. Syrovatskii, 1964, The Origin of Cosmic Rays, Macmillan, NewYork.
[3] A. D. Erlykin, A. W. Wolfendale, J. Phys. G: Nucl. Part. Phys. **23**, 979 (1997).

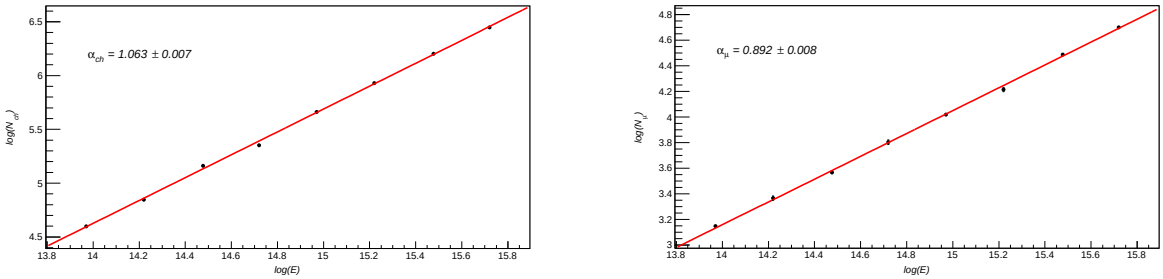

FIG. 3: (Color online) Energy dependence of (a) total charged particles and (b) muon content in proton induced EAS at EASTOP location.

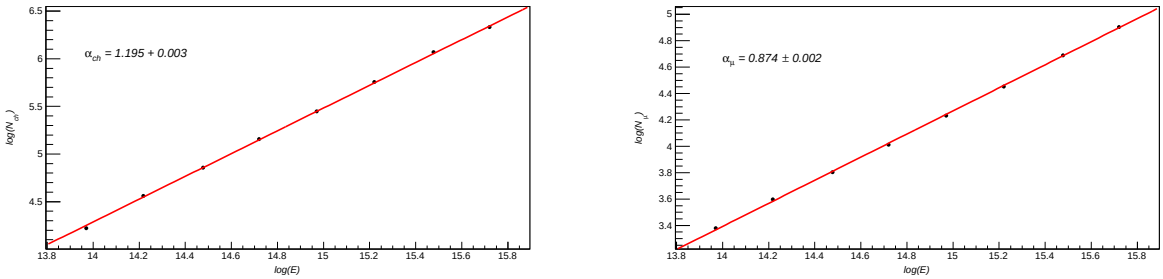

FIG. 4: (Color online) Same as Figure 3 but in Fe initiated EAS .

[4] B. Bijay and A. Bhadra, Res. Astron. Astrophys. (to appear) (2015); eprint arXiv:1412.0818.
[5] G. V. Kulikov, G. B. Khristiansen, JETP, **35**, 441 (1959).
[6] S. I. Nikolsky, and V. A. Romachin, Physics of Atomic Nuclei, **63**, 1799 (2000).
[7] D. Kazanas and A. Nicolaidis, eprint arXiv:astro-ph/0103147 (2001).
[8] Yu. V. Stenkin, Mod. Phys. Lett. **A18** 1225 (2003) .
[9] Yu. V. Stenkin, Nucl. Phys. B (Proc. Suppl.) **151**, 65 (2006)
[10] D M Gromushkin et al., J. Phys. (Conf. Series) **409**, 012044 (2013).
[11] D. Heck, J. Knapp, J. N. Capdevielle, G. Schatz and T. Thouw, Forschungszentrum Karlsruhe Report No. FZKA 6019, (1998).
[12] J. Matthews, Astropart. Phys. **22** 387 (2005).
[13] J. R. Hoerandel, Mod.Phys.Lett.A **22** 1533 (2007)
[14] N. N. Kalmykov, S. S. Ostapchenko and A. I. Pavlov, Nucl. Phys. B, Proc. Suppl. **52** 17 (1997).
[15] M. Bleicher et al., J. Phys. G **25** 1859 (1999).
[16] K. Werner, F. M. Liu and T. Pierog, Phys. Rev. C **74** 044902 (2006).
[17] H. Fesefeldt, RWTH Aachen Report No. PITHA-85/02, (1985).
[18] H. J. Drescher, M. Bleicher, S. Soff and H. Stocker, Astropart. Phys. **21** 87 (2004).
[19] A. Bhadra, S. K. Ghosh, P. S. Joarder, A. Mukherjee and S. Raha, Phys. Rev. D **79** 114027 (2009).
[20] T. Antoni, et.al. (KASCADE collab.), Nucl. Instru. Meth. **513** 490 (2003)
[21] M. Aglietta et al. (EAS-TOP collab.) IL Nuovo Cim. 9C, 262 (1986)
[22] R. Glasstetter et al., Proc. Int. Cosmic Ray Conf. **6**, 157 (1997)
[23] T. Antoni et. al (KASCADE collab.), Astropart. Phys. **16** 373 (2002)
[24] G. Navarra et al (EAS-TOP collab.), Nucl. Phys. B (Proc. Suppl.) 60, 105 (1998)
[25] kcdc.ikp.kit.edu (KIT, Karlsruhe Institute of Technology)

TABLE III: Spectral indices of primary energy spectrum below and above the knee from the electron and the muon size spectra of EAS-TOP observations

Primary before the knee	Primary after the knee	Secondary	$\alpha_{<knee}$	$\alpha_{>knee}$	$\gamma_{<knee}$	$\gamma_{>knee}$	$\Delta\gamma$
Proton	Proton	Electron	1.063 ± 0.007	1.063 ± 0.007	2.71 ± 0.02	3.14 ± 0.07	0.43 ± 0.09
		Muon	0.892 ± 0.008	0.892 ± 0.008	2.89 ± 0.04	3.38 ± 0.09	0.49 ± 0.13
Proton	Iron	Electron	1.063 ± 0.007	1.195 ± 0.003	2.71 ± 0.02	3.40 ± 0.08	0.69 ± 0.10
		Muon	0.892 ± 0.02	0.874 ± 0.002	2.89 ± 0.04	3.33 ± 0.07	0.44 ± 0.11
Iron	Iron	Electron	1.195 ± 0.003	1.195 ± 0.003	2.92 ± 0.02	3.40 ± 0.08	0.48 ± 0.10
		Muon	0.874 ± 0.002	0.874 ± 0.002	2.85 ± 0.03	3.33 ± 0.07	0.48 ± 0.10

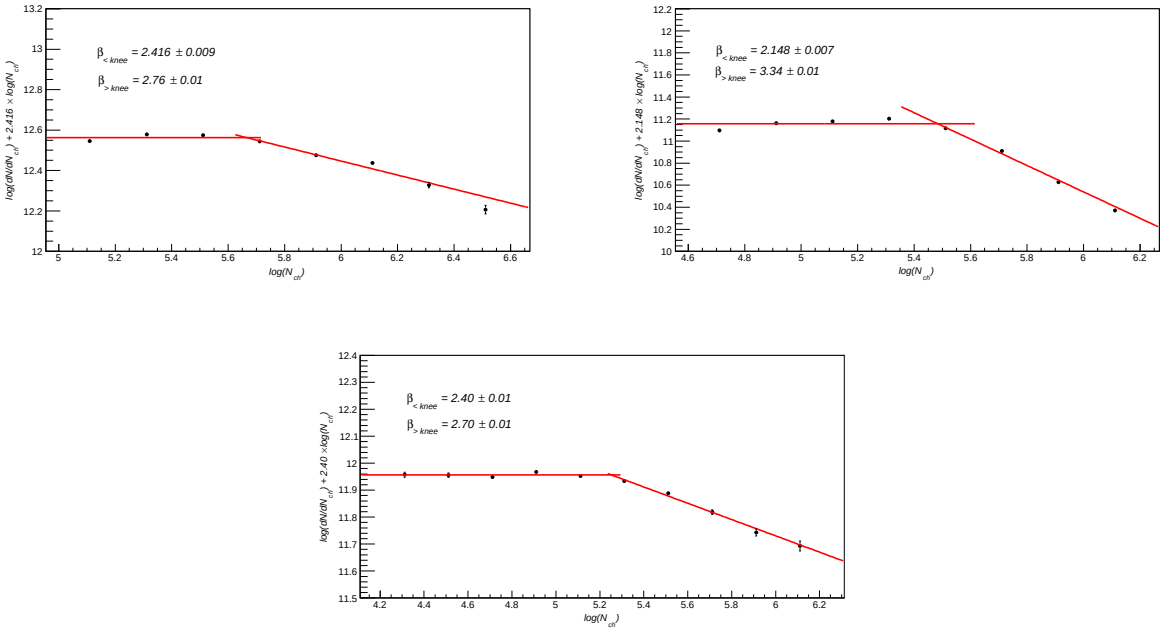

FIG. 5: (Color online) Expected total charged particle size spectrum for different mass composition scenario across the knee (a) unchanged proton primary (b) proton below the knee and Fe above the knee and (c) unchanged Fe primary.

TABLE IV: Spectral indices of the simulated electron and the muon size spectra for cosmic ray energy spectrum with the knee

Primary before the knee	Primary after the knee	Secondary	$\beta_{<knee}$	$\beta_{>knee}$	$\Delta\beta$
Proton	Proton	Electron	2.39 ± 0.01	2.70 ± 0.01	0.31 ± 0.02
		Muon	2.80 ± 0.03	3.30 ± 0.02	0.50 ± 0.05
Proton	Iron	Electron	2.16 ± 0.01	3.03 ± 0.01	0.87 ± 0.02
		Muon	2.86 ± 0.03	3.28 ± 0.02	0.42 ± 0.05
Iron	Iron	Electron	2.40 ± 0.01	2.70 ± 0.01	0.30 ± 0.02
		Muon	2.88 ± 0.02	3.30 ± 0.02	0.42 ± 0.04

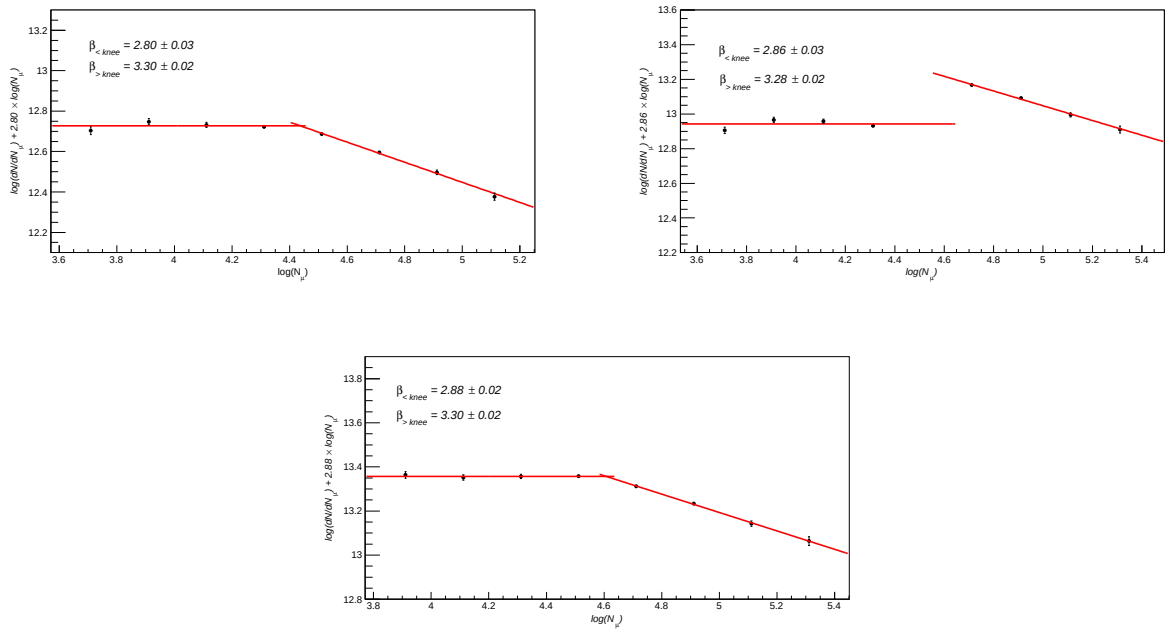

FIG. 6: (Color online) Same as figure 5 but for muon spectrum

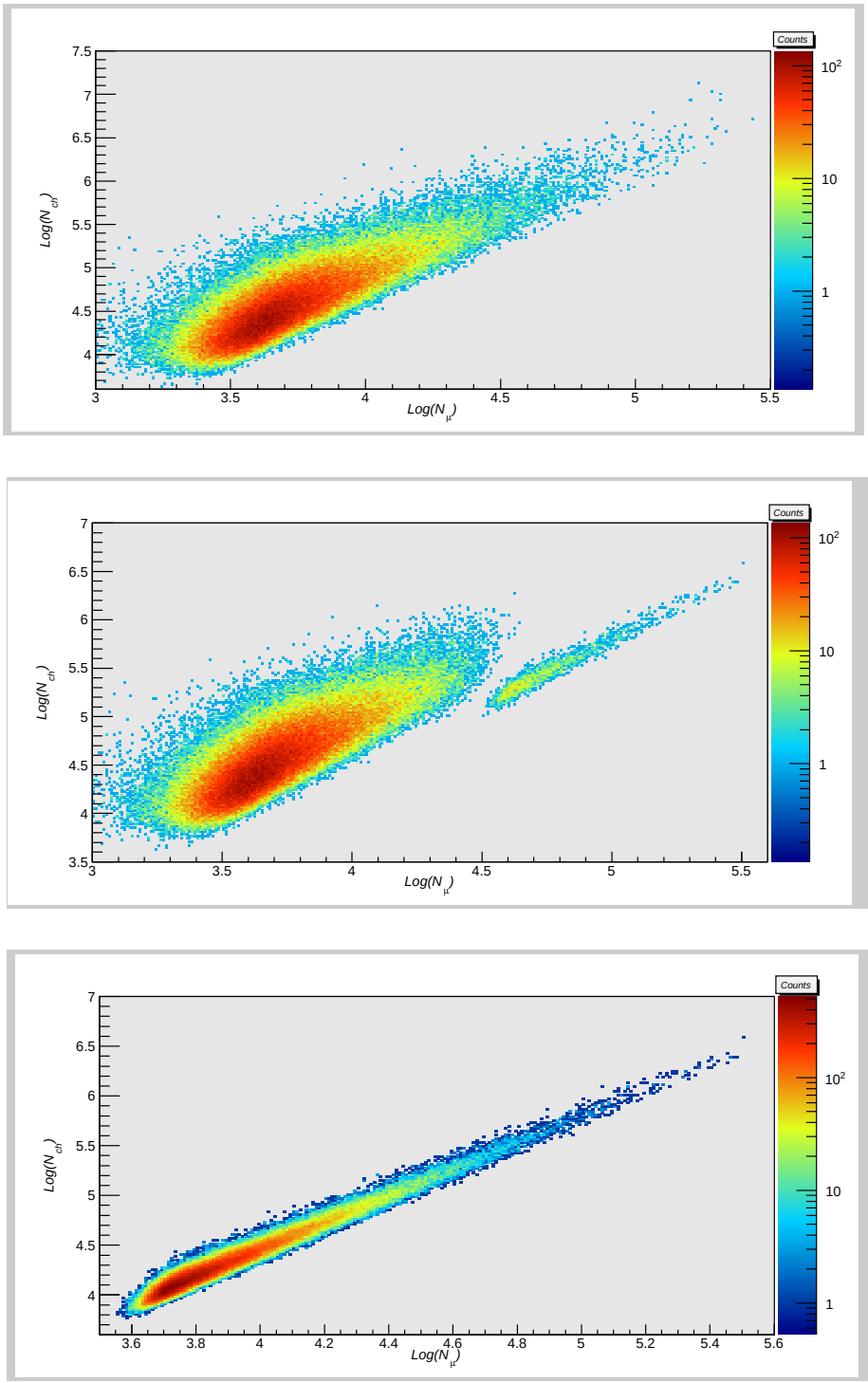

FIG. 7: (Color online) 2-dimentional charged particles - muon spectrum for different composition scenario around the knee

RAA 2015 Vol. **16** No. **1**, 6 (8pp) doi: 10.1088/1674–4527/16/1/006
http://www.raa-journal.org *http://iopscience.iop.org/raa*

Research in Astronomy and Astrophysics

Progenitor model of cosmic ray knee

Biplab Bijay and Arunava Bhadra

High Energy & Cosmic Ray Research Centre, University of North Bengal, Siliguri, WB 734013, India; *aru_bhadra@yahoo.com*

Received 2015 March 07; accepted 2015 July 25

Abstract The primary energy spectrum of cosmic rays exhibits a knee at about 3 PeV where a change in the spectral index occurs. Despite many efforts, the origin of such a feature in the spectrum is not satisfactorily solved yet. Here it is proposed that the steepening of the spectrum beyond the knee may be a consequence of the mass distribution of the progenitor of the cosmic ray source. The proposed speculative model can account for all the major observed features of cosmic rays without invoking any fine tuning to match flux or spectra at any energy point. The prediction of the proposed model regarding the primary composition scenario beyond the knee is quite different from most of the prevailing models of the knee, and thereby can be discriminated from precise experimental measurement of the primary composition.

Key words: cosmic rays — acceleration of particles — black hole physics

1 INTRODUCTION

Ever since their discovery more than a hundred years ago, the origin of cosmic rays has been one of the central questions in physics. But despite many efforts, so far there is no consistent and complete model of the origin of cosmic rays.

The energy spectrum of cosmic rays provides important clues about their origin. The most intriguing feature of the energy spectrum is that although it extends over a wide range of energies, from sub GeV to at least 3×10^{20} eV (the highest energy observed so far), it can be well represented by a steeply falling power law for energies above the solar modulated one. However, the spectrum has a knee around 3 PeV where it steepens sharply as discovered more than half a century ago by Kulikov and Khristiansen of Moscow State University (Kulikov & Khristiansen 1959). The spectrum also has an ankle at an energy of about 3 EeV where it flattens again to its pre-knee slope. It is relatively easier to interpret the flattening of the spectrum above the ankle as the eventual superseding of a harder cosmic ray component which is sub-dominant at lower energies. In contrast, the feature of the knee is more difficult to explain. The existence of the knee in the spectrum is definitely an important imprint of the true model of the origin of cosmic rays and hence a proper explanation of the knee is expected to shed light on the problem of cosmic ray origins.

Several mechanisms have been proposed so far to explain the knee. Shortly after the discovery of the knee, this spectral feature was interpreted as an effect of the reduced efficiency of the galactic magnetic field to confine cosmic ray particles with energies above the knee within the galaxy (Ginzburg & Syrovatskii 1964; Wdowczyk & Wolfendale 1984; Ptuskin et al. 1993; Candia et al. 2002b; Giacinti et al. 2014). Since the magnetic rigidity of a particle is proportional to its atomic number (Z), cosmic ray protons should start escaping first and hence the observed knee is the proton knee as per this model.

The knee has also been explained based on the acceleration mechanism (Fichtel & Linsley 1986; Jokipii & Morfill 1987; Biermann 1993; Berezhko & Ksenofontov 1999; Stanev et al. 1993; Kobayakawa et al. 2002). For reasons of the power required to maintain the observed cosmic ray energy density, it is widely accepted that cosmic rays up to the ankle energy are of galactic origin whereas those having energies above this energy are extragalactic, though there are also suggestions for lower transitional energies (Blasi 2014; Amato 2014; Aloisio et al. 2012). Among the galactic sources, supernova remnants (SNRs) satisfy the energy budget of cosmic rays. The power law behavior of the energy spectrum on the other hand suggests that cosmic rays are most probably energized by diffusive shock acceleration. The maximum energy that a charged particle can gain by diffusive shock acceleration is proportional to Z. The knee has been assigned in this model as the maximum energy that protons can have under diffusive shock acceleration in SNRs.

A critical analysis of data collected at different experiments worldwide in terms of the energy spectrum suggests that the knee is very sharp, and the spectral slope changes rather abruptly at the knee position (Erlykin & Wolfendale 1997). In contrast, the above mentioned rigidity dependent explanations of the knee predict a smooth change in the spectral slope at the knee because of the sum of the contri-

butions of different atomic nuclei having cut-offs at different energies (depending on Z values). To accommodate the sharp knee feature, a few proposals have been advanced. In the single source model the dominant contribution of the cosmic ray flux at the knee is by a nearby source (Erlykin & Wolfendale 1997; Bhadra 2005; Erlykin et al. 2011; Ter-Antonyan 2014) which is superimposed on a galactic modulated component in which the spectral slope is changing smoothly with energy. In another model the sharp knee is explained in terms of cosmic ray acceleration by a variety of supernovae (SNe) (Sveshnikova 2004, 2003). The later proposal relies on the fact that the explosion energy of all SNe is not the same. The sharp knee also could be due to interaction of cosmic ray particles from a pulsar with radiation from the parent SNR (Hu et al. 2009).

The mass composition of cosmic rays will be heavier beyond the knee if the knee is a proton knee. Several Extensive Air Shower (EAS) measurements (till now the study of cosmic rays above 1 PeV has been of an indirect nature via EAS observations) have been made to determine the mass composition of cosmic rays in the energy region of interest, but the measurements have not yielded mutually consistent results yet due to the weak mass resolution of the measured shower observables (Haungs 2011). Most of the findings (Navarra 1998; Glasmacher et al. 1999; Aartsen et al. 2013; Fomin et al. 1996) based on electron content relative to muon content (or *vice versa*) in EAS suggest that composition becomes heavier with energy beyond the knee, though the Haverah Park experiment and a few other observations (particularly underground muon telescopes) (Blake & Nash 1998, 1995; Danilova et al. 1995; Saha et al. 1998; Aglietta et al. 1990; Ahlen et al. 1992; Kasahara et al. 1997; Longley et al. 1995; Bakatanov et al. 1999) found the opposite trend for mass composition. Mass composition estimated from the measurement of the depth of shower maximum through observation of Cerenkov (Boothby et al. 1997; Swordy & Kieda 2000; Fowler et al. 2001; Chernov et al. 2005; Karle et al. 1995; HEGRA-Collaboration et al. 2000; Dickinson 1999; Efimov & et al. 1991) or fluorescence radiation (Abraham et al. 2010; Abbasi et al. 2008, 2004; Tsunesada 2011; Jui & Telescope Array Collaboration 2012), on the other hand, suggests a lighter mass composition beyond the knee differing from that obtained with muon to electron content ratio (Haungs 2011; Hörandel 2013; Bhadra & Sanyal 2005). The mass composition picture of primary cosmic rays is thus still inconclusive in the PeV and higher energy region.

Considering the possibility that mass composition may become lighter beyond the knee, an alternative explanation of the knee was suggested based on nuclear photo-disintegration at the sources (Hillas 1979; Karakula & Tkaczyk 1993; Candia et al. 2002a). In this scenario, heavier components of cosmic rays, particularly Fe nuclei, undergo nuclear photo-disintegration in interactions with the radiation field of the source so that the flux of heavier nuclei decreases with energy beyond the knee whereas protons lose energy by photo-meson production.

A major problem with the standard scenario of diffusive shock acceleration of cosmic rays in SNRs is that a cosmic ray particle can hardly attain the knee energy under this SNR shock acceleration scenario. Such a problem can be overcome in the Cannonball model (Dar & Plaga 1999; Plaga 2002; Dar 2005; de Rújula 2005) in which masses of baryonic plasma or the so called cannonballs, ejected ultra-relativistically in bipolar SN explosions, are considered to be universal sources of hadronic galactic cosmic rays. In this model, the knee corresponds to the maximum energy gained by nuclei through elastic magnetic scattering of ambient particles from the interstellar medium (ISM) in the cannonball while re-acceleration of cosmic rays by cannonballs from other SN explosions causes the extra steepness above the knee.

There is also a proposal of explaining the knee based on a change in the characteristics of high energy interactions (Nikolsky & Romachin 2000). In this model the knee is not a feature of the primary cosmic ray energy spectrum itself, but is caused by the change in high-energy interaction characteristics, either producing a new type of a heavy particle unseen by air shower experiments, or an abrupt increase in the multiplicity of produced particles. However, this proposal has been ruled out at present as the assumed interaction features have not been observed in the Large Hadron Collider experiment.

None of the prevailing models of the knee are free from problems. If the knee corresponds to a break in the proton spectrum, either because it is the maximum energy to which the proton can be accelerated in a galactic cosmic ray source or due to the start of proton leakage from the galaxy at this energy with or without modifications to the sharp knee, then there should be an Fe knee around 10^{17} eV. Hence a special variety of SNe or some other type of galactic or extragalactic source has to be invoked as a generator of cosmic rays between $\sim 10^{17}$ eV and the ankle or galactic-extragalactic transition should occur around 10^{17} eV. The problem with the latter proposal is that it requires fine-tuning to match both the flux and energy at the point where take over occurs. The Cannonball model also suffers the same fine tuning problem at the knee energy. There are other problems such as lower than expected observed gamma ray fluxes from SNRs. The dilemma of the knee thus still continues.

The viable sources of cosmic rays include SNRs, pulsars, gamma ray bursts (GRBs), active galactic nuclei (AGNs), etc. Whatever may be the sources, there is little doubt that they are products of the stellar evolution process. An interesting fact is that the zero age mass spectrum of stars also exhibits power law behavior (Salpeter 1955; Kroupa 2002; Massey et al. 1995). This immediately suggests that the cosmic ray energy spectrum might have some connection with the mass distribution of the progeni-

tor of their sources. In the present work we explore the idea and propose a model for the cosmic ray origin in which the knee of the primary cosmic ray energy spectrum at ~ 3 PeV is a consequence of mass distribution of the progenitor of cosmic ray sources. The proposed model is free from any fine tuning problem and it also overcomes the issue of maximum attainable energy.

The organization of the article is as follows. The model proposed in this work is presented in the next section. The outcome of the present model is discussed in Section 3. The results of the model are compared with observations in Section 4. Finally the results are concluded in Section 5.

2 THE PROPOSED MODEL

Here we propose a model of the origin of cosmic rays in which there is a single class of major cosmic ray sources in the galaxy.

The basic conjectures of the present model are the following:

(1) Cosmic rays, at least up to the ankle energy, are produced either in gravitational explosions (core collapse) of massive stars that lead to formation of black holes (BHs) rather than neutron stars (NSs), or in accretion onto BHs. No other type of galactic or extragalactic source dominates at least up to the ankle energy. Here we have not identified the source. The probable candidate sources of cosmic rays include hypernovae, AGNs and GRBs.
(2) Particles are accelerated by expanding shock waves up to a maximum energy $E_{\rm max}$. The maximum attainable energy $E_{\rm max}$ is, however, not the same for all the sources (of the same kind) but, depending on energy released in explosion/accretion, it has a range. The minimum $E_{\rm max}$ that is possible for cosmic ray sources is equal to the knee energy. We shall argue in the following section that the correspondence of minimum $E_{\rm max}$ with the knee energy is quite plausible and suggestive.

The observed cosmic ray luminosity demands that the cosmic ray sources must be energetically very powerful and are most likely to be powered by gravitational energy. The gravitational collapse that ultimately leads to the formation of a BH or accretion onto a BH is expected to release the maximum gravitational energy. This is the reason for considering the first conjecture. The maximum energy that a cosmic ray particle can attain in shock acceleration usually depends on the explosion energy. Since a BH has no limiting mass, energy released in BH formation should vary with progenitor mass and hence the maximum attainable energies of cosmic ray particles are expected to vary rather than having a fixed value. Essentially, this is the logic behind the second conjecture.

2.1 The Progenitor Connection

Perhaps the occurrence of relativistic shock and non-relativistic shock depends on whether a BH or an NS is formed in the stellar evolution processes. Through stellar core collapse, progenitor stars with $M < 20\ M_\odot$ are supposed to give rise to an NS or white dwarf whereas stars more massive than 20 to 25 $M_\odot$ form a BH (Fryer 1999; Fryer & Heger 2000; Fryer 2003), though such an end point fate also depends on metallicity (Heger et al. 2003). The formation of an NS is usually associated with an SN explosion. The masses of white dwarfs and NSs have to be within the Chandrasekhar limit and Oppenheimer-Volkoff limit respectively. Consequently, the energy released in all ordinary SN explosions is nearly the same. Since a BH has no such upper mass limit, the energy released in the core collapse of massive stars leading to BHs should depend on the mass of the progenitor star.

The gravitational collapse of massive stars to BHs involves some complex, still poorly understood aspects of stellar physics. In the collapsar mechanism (Woosley 1993), a BH is formed when the collapse of a massive star fails to produce a strong SN explosion, leading to its ultimate collapse into a BH. If the stellar material falling back and accreting onto the BH has sufficient angular momentum, it can hang up, forming a disk. This disk, by neutrino annihilation or magnetic fields, is thought to produce the jets which finally results in AGNs or hypernovae.

In the gravitational collapse of a spherical mass distribution with rest mass M leading to formation of a BH, the maximum energy of extraction out of the collapse will be (Ruffini & Vitagliano 2003; Christodoulou & Ruffini 1971),

$$E_{\rm max}^{\rm collapse} = Mc^2/2\,. \qquad (1)$$

During the final stages of stellar evolution, a massive star loses a significant amount of mass. But if a BH is formed, stellar material is likely to fall back and accrete onto the BH (Woosley 1993). The mass of the final produced BH is thus expected to increase linearly with the mass of the progenitor, and hence the distribution of released energy is expected to follow the mass distribution of progenitors.

Instead of a collapse and resulting explosion, a large amount of energy can also be released through the accretion process. The Eddington limit, the maximum steady-state luminosity that can be produced, is given by $L_{\rm ed} = 4\pi GMm_{\rm p}c/\sigma_\tau$ where M is the mass of the BH, $m_{\rm p}$ is the proton mass and σ_τ is the Thomson cross section. The luminosity is thus also proportional to the mass of the BH.

3 OUTCOMES OF THE PROPOSED MODEL

We shall now explore the outcomes of the proposed model regarding the main cosmic ray observables such as luminosity, maximum attainable energy, energy spectrum and nuclear composition.

3.1 The Cosmic Ray Luminosity

The average energy released in BH formation should be around 5×10^{53} erg as per Equation (1), which is more than two orders higher than that released in an SN explosion. Stars more massive than 20 to 25 $M_\odot$ usually form a BH. The rate of stars having $M > 20\ M_\odot$ is $2 \times 10^{-3}\ \mathrm{yr}^{-1}$. However, not all massive stars will end up as BHs. If we denote the probability of BH formation for a star more massive than $20\ M_\odot$ as $\rho_{\rm BH}$, the total energy released in BH production during the cosmic ray confinement period of about 10^6 years in the galaxy is about $\rho_{\rm BH}10^{57}$ erg. This yields a luminosity of $3\rho_{\rm BH}\zeta\times10^{43}$ erg s^{-1}, where ζ is the efficiency of conversion of explosion energy into cosmic ray energy. Typically ζ ranges from 0.01 to 0.1 whereas $\rho_{\rm BH}$ may be taken as 0.5 (Clausen et al. 2015).

3.2 The Maximum Attainable Energy

The maximum energy that a particle with charge Ze can attain in a bulk magnetized flow on a scale $R_{\rm s}$, with velocity $c\beta_{\rm s}$ and magnetic field B, is (Hillas 1984)

$$E_{\rm max} = ZeB\Gamma_{\rm s}\beta_{\rm s}R_{\rm s}\,, \tag{2}$$

where $\Gamma_{\rm s}$ is the Lorentz factor of the relativistic shock wave. This value of $E_{\rm max}$ is a factor $\Gamma_{\rm s}$ larger than that obtained from the Hillas condition. In a BH formation scenario, a fraction of all kinetic energy carries debris ejected with the largest Lorentz factor, thereby generating gamma ray emission in the form of a burst, but the bulk of ejecta is less relativistic or even sub-relativistic. Note that if $\sim 10\ M_\odot$ is given $\sim 10^{54}$ erg then the typical velocity of the mass would be 10^{10} cm, i.e. $c/3$. GRBs are likely to occur in BH formation collapse and a hint on typical values of $\Gamma_{\rm s}$ may be found from GRBs. The GRB observations suggest the minimum $\Gamma_{\rm s}$ of the burst is a few tens (Racusin et al. 2011; Lithwick & Sari 2001; Zou et al. 2011). Therefore, the minimum $E_{\rm max}$ for a BH producing an explosion should be a few PeV.

Let us consider a more rigorous description. In the standard scenario the acceleration of cosmic rays occurs at (non-relativistic) shocks of isolated SNRs. The maximum energy that can be attained by a cosmic ray particle in an ordinary SNR when the remnant is passing through a medium of density $N_{\rm H}\ \mathrm{cm}^{-3}$ is (Fichtel & Linsley 1986; Biermann 1993; Berezhko & Ksenofontov 1999)

$$E_{\rm max} \simeq 4\times10^5 Z \left(\frac{E_{\rm SN}}{10^{51}\ \mathrm{erg}}\right)^{1/2} \left(\frac{M_{\rm ej}}{10\ M_\odot}\right)^{-1/6} \left(\frac{N_{\rm H}}{3\times10^{-3}\ \mathrm{cm}^{-3}}\right)^{-1/3} \left(\frac{B_{\rm o}}{3\mu G}\right)\ \mathrm{GeV}\,, \tag{3}$$

which falls short of the knee by about one order of magnitude. Energy released in BH formation explosions is at least two orders higher than that in SN explosions. Moreover, as stated before, for relativistic shock acceleration $E_{\rm max}$ will be a factor $\Gamma_{\rm s}$ higher. Hence the minimum $E_{\rm max}$ for an explosion that produces a BH should be a few PeV.

An important question for such an explosion that forms a BH in terms of the origin of cosmic rays is whether or not $E_{\rm max}$ could reach the ankle energy. Unlike the almost constant energy released in SN explosions, energy output in such a scenario varies and it may increase at least two orders higher than its minimum value. Such high energy events are expected to occur in a more rarefied medium. Hence it is very likely that the maximum $E_{\rm max}$ will exceed the ankle energy.

Interestingly, the AGN minimum $E_{\rm max}$ is about 3 PeV (Stecker et al. 1991) which is the knee energy and the maximum $E_{\rm max}$ can be many orders higher than that owing to the wide range of luminosities of AGNs.

3.3 Energy Spectrum

In the proposed model, cosmic rays are accelerated in diffusive relativistic shock acceleration. The energy spectrum of accelerated particles in each source is, therefore, given by a power law

$$\frac{dn}{dE} = AE^{-\gamma}\,, \tag{4}$$

with γ around 2.2, and A the normalization constant

$$A \equiv \frac{\epsilon}{(\gamma-2)(E_{\rm min}^{-\gamma+2} - E_{\rm max}^{-\gamma+2})}\,, \tag{5}$$

where $E_{\rm min}$ and $E_{\rm max}$ are respectively the minimum and maximum attainable energies of cosmic ray particles in the source.

The sources do not all have the same $E_{\rm max}$. Above the minimum possible $E_{\rm max}$, which we denote as $E_{\rm max}^{\rm min}$, the spectrum will be modified due to the distribution of $E_{\rm max}$. To get the spectrum beyond $E_{\rm max}^{\rm min}$ we need to obtain the maximum energy distribution of the cosmic ray sources from the mass distribution of their progenitors. The calculation involves a sequence of steps. Using the expression for explosion energy as a function of progenitor mass as obtained in the previous section, we convolve the resulting explosion energy-progenitor mass relation with the initial mass function of the progenitors to obtain the explosion energy distribution. Subsequently using the relation of maximum energy that a cosmic ray particle may attain in the relativistic shock acceleration process with explosion energy, we derive the maximum energy distribution for main cosmic ray sources. Using such a distribution we obtain the energy spectrum of cosmic rays beyond the $E_{\rm max}^{\rm min}$.

The stellar initial mass function, or distribution of masses with which stars are formed, can be represented by a declining power law

$$\frac{dn}{dM} \propto M^{-\alpha}\,, \tag{6}$$

with the universal (Salpeter) value of the exponent $\alpha = -2.35$ over the whole mass range above 3 $M_\odot$ (Salpeter 1955; Kroupa 2002; Massey et al. 1995). Since explosion energy (ϵ) scales linearly with M, the expected explosion energy distribution of massive progenitor stars is also represented by $\frac{dn}{d\epsilon} \propto \epsilon^{-\alpha}$.

The Lorentz factor of a relativistic shock is nearly equal to the initial Lorentz factor of the jet, i.e. $\Gamma_{\rm s} \sim \gamma_o$. The relativistic shock waves must carry a significant fraction of the explosion energy which is subsequently converted to energies of cosmic rays. Hence, $\Gamma_{\rm s}$ should be proportional to explosion energy. On the other hand, $E_{\rm max}$ is also proportional to $\Gamma_{\rm s}$. So for the proposed model, $E_{\rm max} \propto \epsilon$. Thus we have

$$\frac{dn}{dE_{\rm max}} \propto E_{\rm max}^{-\alpha}\,. \tag{7}$$

Therefore, the number of sources having $E_{\rm max} \geq E$ is $j(E_{\rm max} \geq E) \propto E_{\rm max}^{-\alpha+1}$. As the minimum $E_{\rm max}$ of a source is equal to $E_{\rm max}^{\rm min}$, all such sources will contribute to cosmic ray flux when cosmic ray energy is below or equal to $E_{\rm max}^{\rm min}$. However, for energies above $E_{\rm max}^{\rm min}$ ($E > E_{\rm max}^{\rm min}$), only sources having $E_{\rm max} \geq E$ will contribute. The resultant cosmic ray spectrum above $E_{\rm max}^{\rm min}$ will be

$$\frac{dn}{dE} = \int_E \frac{dn}{dE_{\rm max}} A E^{-\gamma} dE_{\rm max} \propto E^{-\gamma-\alpha+2}\,. \tag{8}$$

Therefore, beyond $E_{\rm max}^{\rm min}$ the spectrum should steepen by 0.35 in spectral index as observed. Note that the difference in the exponent of energy by one between the above equation and Equation (3) of Kachelrieß & Semikoz (2006). There the power law distribution of the maximum attainable energy of sources was assumed, due to the fact that our normalization constant A is proportional to the explosion energy (and hence to the maximum attainable energy), unlike the normalization constant that is independent of explosion energy that was adopted in Kachelrieß & Semikoz (2006).

3.4 Mass Composition

According to the proposed model, cosmic rays below and just above $E_{\rm max}^{\rm min}$ are produced in explosions that form a BH comparable to the progenitor's mass. Hence there should not be any abrupt change in mass composition through the $E_{\rm max}^{\rm min}$. In this model, higher energy particles originate from the sources with heavier progenitors. Since a BH is the last stage of evolution for massive stellar objects, the composition is unlikely to change much for BHs from heavier progenitors. Therefore, the resulting composition of accelerated cosmic rays in the proposed model is expected to remain almost unaltered with energy or may become slightly heavier at higher energies.

4 DISCUSSION

We shall now compare the outcomes of the proposed model against the observational features of cosmic rays.

The conventional estimate of cosmic ray luminosity in our galaxy is $\sim 5 \times 10^{40}$ erg s^{-1}. As shown in the previous section, the proposed model yields a cosmic ray luminosity equal to $3\rho_{\rm BH}\zeta \times 10^{43}$ erg s^{-1}. Typically ζ ranges from 0.01 to 0.1 whereas $\rho_{\rm BH}$ is around 0.5 (Clausen et al. 2015). Therefore, the power from explosions that produce BHs in the galaxy satisfies the power requirement for accelerating all galactic cosmic rays. Note that with the rate of occurrence of one per thirty years and the average energy released in each SN explosion of around 10^{51} erg, SNRs satisfy the energy budget for observed cosmic rays (and hence are favored as the main source of cosmic rays) provided the energy conversion efficiency parameter ζ is relatively higher, around 0.1 to 0.2.

The maximum energy that can be attained by a cosmic ray particle in relativistic shock acceleration under the framework of the proposed model varies from source to source (of the same kind). Because of the relativistic effect (through the Lorentz factor) and owing to the much larger explosion energy, the minimum $E_{\rm max}$ for cosmic rays is found to equal a few PeV as shown in the previous section, which can be identified as the knee energy. Interestingly, the minimum $E_{\rm max}$ for an AGN is about 3 PeV (Stecker et al. 1991), whereas the maximum $E_{\rm max}$ is found to exceed even the ankle energy. So, the maximum attainable energy requirement is satisfied in a generic way. In contrast, the maximum energy that can be attained by a cosmic ray particle in an ordinary SNR is 0.3 PeV which falls short of the knee by about one order of magnitude unless the idea of magnetic amplification is invoked. Even with magnetic amplification, it is difficult to exceed 100 PeV and thereby a new source with an unknown nature is required between 100 PeV and the ankle energy.

Since the proposed model relies on standard shock acceleration theory, the overall cosmic ray production spectrum will follow a power law behavior with spectral index equal to –2.2. Due to diffusive propagation of cosmic rays through the ISM, the slope of the spectrum recorded at Earth should steepen to ~ 2.7 till the knee of the spectrum, and the knee should be as sharp as observed. Above the knee, the spectrum will be modified by 0.35 due to the distribution of $E_{\rm max}$ as demonstrated in Section 3.3. Thus

the proposed model explains well the observed features of the energy spectrum of primary cosmic rays.

With respect to the mass composition of cosmic rays, particularly above the knee energy, the composition predicted by the model is similar to that of the Cannonball model but different from the prediction of the SN model that has a cosmic ray origin.

Very recent findings by the KASCADE-GRANDE collaboration regarding the existence of an Fe-knee around 80 PeV along with the composition scenario that is dominated by heavier particles (Apel et al. 2013, 2012, 2011), together with earlier results of the KASCADE experiment for a proton knee at 3 PeV (Apel et al. 2009), do not support the composition picture predicted by the proposed model. Importantly in the overlapping energy region around 1 EeV, the composition scenario inferred from the KASCADE-GRANDE or ICETOP findings, with a mixed composition having nearly the same contribution from protons and iron nuclei (Apel et al. 2009), is not in agreement with a proton dominated chemical composition that emerged from observations at the Pierre Auger Observatory (Abraham et al. 2010), HiRes (Abbasi et al. 2008, 2004) and Telescope Array (Tsunesada 2011; Jui & Telescope Array Collaboration 2012). This only shows the difficulty in estimating primary masses from air shower experiments that rest on comparisons of data with EAS simulations where the latter requires hadronic interaction models as input, which are still uncertain to a large extent at present. Moreover, the uniqueness of solutions of primary energy spectra in the knee region from EAS data is also questioned (Ter-Antonyan 2007). It is expected that the mass composition scenario predicted by the present model will motivate newer experiments, exploiting both muon to electron content ratio and optical techniques, to establish unambiguous cosmic ray mass composition in the knee region and in particular to confirm the KASCADE-Grande results including the Fe-knee.

An important question is to identify the sources, or more precisely identifying the gravitational explosions, that lead to formation of BHs. The viable galactic sources resulting in BH formation include Type 1b/1c SNe and hypernovae, whereas GRBs and AGNs seem to be possible extragalactic sources. The observed rate of Type 1b and 1c SNe is around $10^{-3}\ \mathrm{yr}^{-1}$ which is close to the rate of stars having mass greater than $20\ M_{\odot}$. Radio observations suggest that about 5% of Type 1b/1c SNe can be produced in GRBs (Berger et al. 2003). Earlier, Sveshnikova demonstrated that hypernovae can satisfy the power requirement for accelerating all galactic cosmic rays (Sveshnikova 2004) assuming the rate of hypernovae is about $10^{-4}\ \mathrm{yr}^{-1}$. The extragalactic origin of cosmic rays is usually considered to be unlikely on energetic grounds. However, such a problem can be circumvented by employing the flux trapping hypothesis as proposed in (Plaga 1998; Burbidge 1962). Hence the possibility of a GRB/AGN as the sole kind of dominant source of cosmic rays cannot be totally ruled out from an energetic consideration.

5 CONCLUSIONS

In summary, the proposed speculative BH based model of the origin of cosmic rays can account for all the major observed features of cosmic rays without any serious contradiction to observational results. The knee of the energy spectrum has been ascribed as a consequence of the mass distribution of the progenitor of the cosmic ray source. Such a philosophy seems applicable to the Cannonball model of cosmic ray origin, replacing the original proposal of second order Fermi acceleration of cosmic rays by Cannonballs of other SN explosions as the cause of spectral steepening above the knee (Dar & Plaga 1999; Plaga 2002; Dar 2005; de Rújula 2005). Precise measurement of the primary mass composition can be used to discriminate the proposed model from most of the standard prevailing models of the cosmic ray knee. No definite cosmic ray sources could be identified at this stage within the framework of the proposed model, which would be an important future task for further development of the proposed model.

Acknowledgements The authors are grateful to an anonymous reviewer for insightful comments and suggestions that helped us to improve the manuscript. AB thanks Professors C. L. Fryer and S. E. Woosley for helpful discussions. This work is partly supported by the Department of Science and Technology (Govt. of India) under the grant no. SR/S2/HEP-14/2007.

References

Aartsen, M. G., Abbasi, R., Abdou, Y., et al. 2013, Phys. Rev. D, 88, 042004

Abbasi, R. U., Abu-Zayyad, T., Amann, J. F., et al. 2004, Physical Review Letters, 92, 151101

Abbasi, R. U., Abu-Zayyad, T., Allen, M., et al. 2008, Physical Review Letters, 100, 101101

Abraham, J., Abreu, P., Aglietta, M., et al. 2010, Physical Review Letters, 104, 091101

Aglietta, M., Badino, G., Bologna, G., et al. 1990, Nuclear Physics B Proceedings Supplements, 14, 193

Ahlen, S., Ambrosio, M., Antolini, R., et al. 1992, Phys. Rev. D, 46, 4836

Aloisio, R., Berezinsky, V., & Gazizov, A. 2012, Astroparticle Physics, 39, 129

Amato, E. 2014, International Journal of Modern Physics D, 23, 30013

Apel, W. D., Arteaga, J. C., Badea, A. F., et al. 2009, Astroparticle Physics, 31, 86

Apel, W. D., Arteaga-Velázquez, J. C., Bekk, K., et al. 2011, Physical Review Letters, 107, 171104

Apel, W. D., Arteaga-Velázquez, J. C., Bekk, K., et al. 2012, Astroparticle Physics, 36, 183

Apel, W. D., Arteaga-Velàzquez, J. C., Bekk, K., et al. 2013, Phys. Rev. D, 87, 081101
Arqueros, F., HEGRA-Collaboration 2000, A&A, 359, 682
Bakatanov, V. N., Novosel'tsev, Y. F., & Novosel'tseva, R. V. 1999, Astroparticle Physics, 12, 19
Berezhko, E. G., & Ksenofontov, L. T. 1999, Soviet Journal of Experimental and Theoretical Physics, 89, 391
Berger, E., Kulkarni, S. R., Frail, D. A., & Soderberg, A. M. 2003, ApJ, 599, 408
Bhadra, A. 2005, International Cosmic Ray Conference, 3, 117
Bhadra, A., & Sanyal, S. 2005, International Cosmic Ray Conference, 6, 137
Biermann, P. L. 1993, A&A, 271, 649
Blake, P. R., & Nash, W. F. 1995, Journal of Physics G Nuclear Physics, 21, 1731
Blake, P. R., & Nash, W. F. 1998, Journal of Physics G Nuclear Physics, 24, 217
Blasi, P. 2014, Comptes Rendus Physique, 15, 329
Boothby, K., Chantell, M., Green, K. D., et al. 1997, ApJ, 491, L35
Burbidge, G. 1962, Progress of Theoretical Physics, 27, 999
Candia, J., Epele, L. N., & Roulet, E. 2002a, Astroparticle Physics, 17, 23
Candia, J., Roulet, E., & Epele, L. N. 2002b, Journal of High Energy Physics, 12, 33
Chernov, D. V., Korosteleva, E. E., Kuzmichev, L. A., et al. 2005, International Journal of Modern Physics A, 20, 6799
Christodoulou, D., & Ruffini, R. 1971, Phys. Rev. D, 4, 3552
Clausen, D., Piro, A. L., & Ott, C. D. 2015, ApJ, 799, 190
Danilova, E. V., Kabanova, N. V., Nikolsky, S. I., Romakhin, V. A., & Lebedev, P. N. 1995, 24th International Cosmic Ray Conference, 1, 285
Dar, A. 2005, Nuovo Cimento B Serie, 120, 767
Dar, A., & Plaga, R. 1999, A&A, 349, 259
de Rújula, A. 2005, International Journal of Modern Physics A, 20, 6562
Dickinson, J. E. 1999, International Cosmic Ray Conference, 3, 136
Efimov, N. N., & et al. 1991, in Astrophysical Aspects of the Most Energetic Cosmic Rays, ed. M. Nagano & F. Takahara, 20
Erlykin, A. D., & Wolfendale, A. W. 1997, Journal of Physics G Nuclear Physics, 23, 979
Erlykin, A. D., Martirosov, R., & Wolfendale, A. W. 2011, CERN Courier, 51, 21
Fichtel, C. E., & Linsley, J. 1986, ApJ, 300, 474
Fomin, Y. A., Kalmykov, N. N., Khristiansen, G. B., et al. 1996, Journal of Physics G Nuclear Physics, 22, 1839
Fowler, J. W., Fortson, L. F., Jui, C. C. H., et al. 2001, Astroparticle Physics, 15, 49
Fryer, C. L. 1999, ApJ, 522, 413
Fryer, C. L., & Heger, A. 2000, ApJ, 541, 1033
Fryer, C. L. 2003, Classical and Quantum Gravity, 20, 73
Giacinti, G., Kachelrieß, M., & Semikoz, D. V. 2014, Phys. Rev. D, 90, 041302
Ginzburg, V. L., & Syrovatskii, S. I. 1964, The Origin of Cosmic Rays (New York: Macmillan)
Glasmacher, M. A. K., Catanese, M. A., Chantell, M. C., et al. 1999, Astroparticle Physics, 12, 1
Haungs, A. 2011, Astrophysics and Space Sciences Transactions, 7, 295
Heger, A., Fryer, C. L., Woosley, S. E., Langer, N., & Hartmann, D. H. 2003, ApJ, 591, 288
Hillas, A. M. 1979, International Cosmic Ray Conference, 8, 7
Hillas, A. M. 1984, ARA&A, 22, 425
Hörandel, J. R. 2013, in American Institute of Physics Conference Series, 1516, ed. J. F. Ormes, 185
Hu, H.-B., Yuan, Q., Wang, B., et al. 2009, ApJ, 700, L170
Jokipii, J. R., & Morfill, G. 1987, ApJ, 312, 170
Jui, C. C. H., & Telescope Array Collaboration. 2012, Journal of Physics Conference Series, 404, 012037
Kachelrieß, M., & Semikoz, D. V. 2006, Physics Letters B, 634, 143
Karakula, S., & Tkaczyk, W. 1993, Astroparticle Physics, 1, 229
Karle, A., Merck, M., Plaga, R., et al. 1995, Astroparticle Physics, 3, 321
Kasahara, S. M., Allison, W. W., Alner, G. J., et al. 1997, Phys. Rev. D, 55, 5282
Kobayakawa, K., Honda, Y. S., & Samura, T. 2002, Phys. Rev. D, 66, 083004
Kroupa, P. 2002, Science, 295, 82
Kulikov, G. V., & Khristiansen, G. B. 1959, Soviet Physics JETP, 35, 441
Lithwick, Y., & Sari, R. 2001, ApJ, 555, 540
Longley, N. P., Bode, C. R., Border, P. M., et al. 1995, Phys. Rev. D, 52, 2760
Massey, P., Johnson, K. E., & Degioia-Eastwood, K. 1995, ApJ, 454, 151
Navarra, G. 1998, Nuclear Physics B Proceedings Supplements, 60, 105
Nikolsky, S. I., & Romachin, V. A. 2000, Physics of Atomic Nuclei, 63, 1799
Plaga, R. 1998, A&A, 330, 833
Plaga, R. 2002, New Astron., 7, 317
Ptuskin, V. S., Rogovaya, S. I., Zirakashvili, V. N., et al. 1993, A&A, 268, 726
Racusin, J. L., Oates, S. R., Schady, P., et al. 2011, ApJ, 738, 138
Ruffini, R., & Vitagliano, L. 2003, International Journal of Modern Physics D, 12, 121
Saha, G., Bhadra, A., Chakrabarti, C., Sarkar, S. K., & Chaudhuri, N. 1998, Nuovo Cimento C Geophysics Space Physics C, 21, 215
Salpeter, E. E. 1955, ApJ, 121, 161
Stanev, T., Biermann, P. L., & Gaisser, T. K. 1993, A&A, 274, 902

Stecker, F. W., Done, C., Salamon, M. H., & Sommers, P. 1991, Physical Review Letters, 66, 2697
Sveshnikova, L. G. 2003, A&A, 409, 799
Sveshnikova, L. G. 2004, Astronomy Letters, 30, 41
Swordy, S. P., & Kieda, D. B. 2000, Astroparticle Physics, 13, 137
Ter-Antonyan, S. 2014, Phys. Rev. D, 89, 123003
Ter-Antonyan, S. V. 2007, Astroparticle Physics, 28, 321
Tsunesada, Y. 2011, International Cosmic Ray Conference, 12, 67 (arXiv:1111.2507)
Wdowczyk, J., & Wolfendale, A. W. 1984, Journal of Physics G Nuclear Physics, 10, 1453
Woosley, S. E. 1993, ApJ, 405, 273
Zou, Y.-C., Fan, Y.-Z., & Piran, T. 2011, ApJ, 726, L2